Liquid-Induced Discharge of Polypropylene Microfiber Electret Filters

Thesis by
Albert Isaac Nazeeri

In Partial Fulfillment of the Requirements for the
Degree of
Bachelor of Science in Physics

CALIFORNIA INSTITUTE OF TECHNOLOGY
Pasadena, California

2021
Defended 2 June 2021

Albert Isaac Nazeeri
ORCID: 0000-0003-0000-9841

Acknowledgements

This thesis would not have been possible without the support, generosity, and guidance of Professor Joseph Kirschvink, my thesis advisor, throughout the past year and a half. The Kirschvink lab has been a fantastic research environment and I have learned a great deal about the scientific profession from the members of the Kirschvink group.

I am grateful for the support Isaac Hilburn has provided me in this thesis work, especially for his assistance with materials procurement and his help with debugging LabVIEW device drivers.

I am thankful for the many people who have provided feedback on my work including Dr. Daw-An Wu, Yovan Badal, Kabir Mohammed, Professor Moses Chan, and Professor Richard Flagan.

I am also grateful for the filtration efficiency data Dr. Buddhi Pushpawela has collected on my behalf using the Flagan group's polydispersed NaCl aerosol filter testing device. Finally, I am grateful for the love and support of my parents and family.

Abstract

Polymer microfiber electret filters are the technology behind N95 and equivalent type respirators. Understanding how liquids interact with and discharge these filters would allow for the development of non-damaging liquid decontamination protocols. Previous work on liquid/filter interactions has been largely empirical with articles reporting the effect a specific liquid has on the filtration efficiency of a particular filter. This thesis proposes a theoretical model of liquid induced discharge of polymer microfiber electret filters via the ideas of surface wetting and electrical conductivity. This model was tested, and validated, on commercially available polypropylene microfiber electret filters through wetting, thermally stimulated discharge (TSD), and filtration experiments.

Table of Contents

Chapter I: Introduction

1.1 Polymer Microfiber Electret Filters

Polymer microfiber electret filters are the technology behind N95 and equivalent type respirators. The fibers in these filters are charged in a manner that allows micron sized fibers to efficiently remove aerosol particulates from air, with little pressure drop across the filters [1]. This charge on the fibers is important to filtration, especially in the 50 to 500 nm particle diameter regime where electrostatic collection contributes a large fraction to a microfiber filter's filtration efficiency [2]. As the microfibers in N95 and similar type respirators are fashioned out of very low conductivity polymers, the charge in these filters takes many years to discharge [3][4]. This long timescale for the microfiber electret discharge is in contrast with the typical single use of an N95 respirator. The primary limitation to the reuse of N95 respirators, especially in a medical environment, is contamination of the device. Over the past two decades, a volume of literature has grown around quantifying possible N95/polymer microfiber electret filter decontamination techniques [5][6][7] [8].

The Covid-19 pandemic over the past year caused a large increase in the demand for N95 and similar type respirators. This crisis prompted many papers on possible methods on decontaminating N95 respirators for reuse, and initial work on this thesis was inspired by this cohort of decontamination articles [9][10][11]. This thesis focuses on liquid-based decontamination methods as liquids, unlike other popular approaches to decontamination like UV light and hydrogen peroxide vapor, can potentially remove debris from the filter. Furthermore, the literature on liquid decontamination has reported some successes with water [5] [7], dilute bleach solution [5][6], and 3-6% hydrogen peroxide solution [5][6]. There have also been many reported failures, with liquid treatments drastically reducing filtration performance. Notable examples include ethanol, acetone, and isopropyl alcohol solutions [5][7][8][9][10][11][12].

One thing lacking in the literature is an agreed upon theory for when a liquid will damage a microfiber electret filter. Work in this thesis was done in the pursuit of developing and testing such a theory.

1.2 Literature Review of Liquid Decontamination Results

An interesting pattern in the filtration data emerges when one arranges the treatment solutions in terms of their surface tensions. Figure 1.1 shows the filtration damages reported in the literature for specific liquid/polypropylene microfiber electret filter interactions, plotted against the surface tension of the liquid treatment. Several things are apparent from this figure: the high surface tension solutions (dilute bleach, 3-6% hydrogen peroxide, water) all did minimal damage, the low surface tension solutions (ethanol, acetone, and IPA) had highly variable results, and a large range of surface tension values (30-70 mN/m) have not yet been investigated.

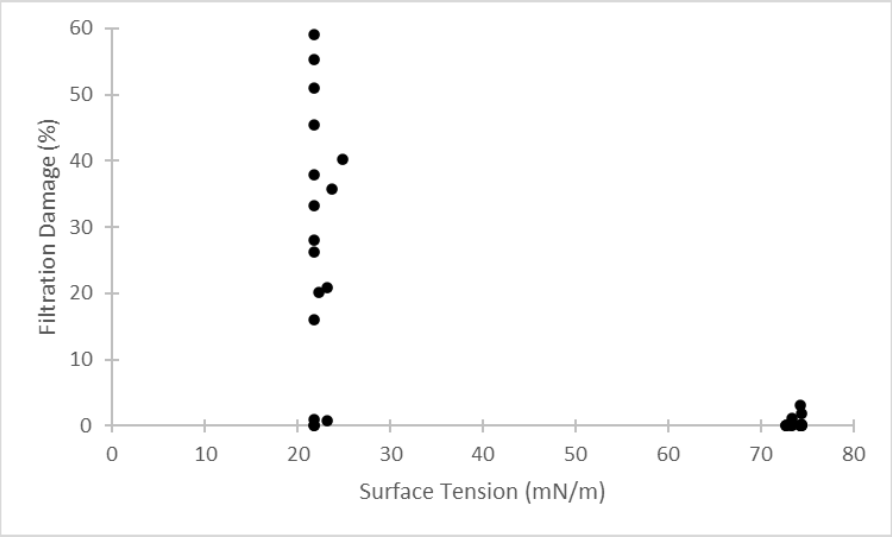

Figure 1.1 Literature reported filtration damage versus treatment solution surface tension for various polypropylene microfiber electret filters. The low surface tension data points include ethanol, acetone, and isopropyl alcohol solutions. The high surface tension data points include 0.5-0.6% bleach solutions, 3-6% hydrogen peroxide solutions, and water. Filtration data was taken from [6][7][8][9][10][11][12]. Surface tension data was taken from [13][14][15][16].

1.3 Overview of Thesis

The aim of this thesis is to develop and test a theory of liquid induced discharge of polymer microfiber electret filters. A theory of this is developed in chapter 2 using the ideas of surface wetting and the electrical conductivity of liquids and insulators. The wetting theory developed in that chapter predicts two separate wetting transitions for a nonwoven microfiber network with rough microfibers, corresponding to liquid penetrating into the network of microfibers, and then fully wetting into the rough surfaces of individual fibers.

Chapter 3 presents results from several wetting experiments, applying a series of ethanol/water solutions to the polypropylene microfiber electret filters from 3M 8210 N95 respirators. These experiments verified the first transition predicted by the surface tension/wetting theory.

In chapter 4, the thermally stimulated discharge (TSD) technique is introduced, and a brief theoretical background is given. A TSD device was built for this thesis, and details on the design and fabrication of the device are given. The TSD device was used to analyze the effect different liquid treatments had on the electret state in polypropylene microfiber electret filters sourced from 3M 8210 N95 respirators. These results were related to the wetting and discharge theory developed in chapter 2.

Chapter 5 presents preliminary filtration efficiency data gathered on 3M 8210 N95 respirators subjected to different liquid treatments using the Flagan group's polydispersed NaCl aerosol filtration testing device. This filtration data was then correlated with the filter's electret state data from the previous chapter. These results supported the wetting and discharge theory developed in chapter 2.

Finally, this thesis concludes with a discussion of potential applications of the theory developed and results obtained in this work.

Chapter II: Theory of Liquid-Induced Microfiber Electret Discharge

This chapter develops a theory of liquid-polymer microfiber electret discharge, via the ideas of surface wetting and electrical conductivity in liquids and insulators.

2.1 Liquids and Polymer Microfiber Electret Filters

Electret filters work by storing a charge distribution (excess charge or a polarization) in an insulator. For commercial electret filters, highly resistive polymers like polypropylene (~10^{14} Ωm) are chosen as these materials can hold useful amounts of charge for decades: Sessler estimates the dielectric relaxation time for nonpolar polymer electrets at approximately 10^9 seconds or around 30 years [4][17].

This stability of the electret state in polypropylene reflects the lack of mobile charge carriers in the material; charge is instead held in a bunch of traps throughout the material. Polypropylene is a semi-crystalline polymer, so the properties of the trapping sites are intimately related to the properties of the polymer spherulites. In bulk polypropylene, the stability of the electret state was found by Thyssen to be inversely correlated with the spherulite size [18]. Thyssen also found that the size of the spherulites was proportional to the cooling time, with the quickest cooled samples having spherulites approximately 0.7 μm in size. In general, it would be expected that a polypropylene microfiber would cool faster than bulk polypropylene, so presumably the spherulites in a filter microfiber should be at or below 0.7 μm in size.

The proposed mechanism for discharging a polymer microfiber electret is the conductivity of the applied fluid. Most fluids, even in a very pure form, are many orders of magnitude more conductive than the polymers used in electret filters like polypropylene (Table 2.1). An important constraint to this liquid induced discharge is the very low charge mobility in these polymers. The primary mode of charge movement (and non-liquid induced discharge) is hopping or tunnelling from trapping site to trapping site; this implies that for reasonable time scales, a liquid should only be able to access, and discharge, the first layer of trapping sites near a solid-liquid interface.

Table 2.1. Resistivity of relevant materials

Material	Resistivity (Ωm)	Source
Pure Water	$1.8 \cdot 10^5$	[19]
Pure Ethanol	$2.0 \cdot 10^8$	[19]
Polypropylene	$2.4 \cdot 10^{14}$	[17]

Assuming discharge is dependent on a solid-liquid interface, the importance of wetting to the discharge of a polymer microfiber electret filter becomes apparent. In this thesis, the model filter was the polypropylene microfiber electret filter from a 3M 8210 N95 respirator. Image data on this specific filter suggests that the wetting problem for polypropylene electret filters should be understood at two different length scales: wetting of single microfibers (Fig. 2.1) and wetting of the nonwoven microfiber network (Fig. 2.2). This is justified as the wetting of the nonwoven microfiber network is a prerequisite for wetting the microfibers, but as the individual microfibers

are rough and porous, complete wetting of the microfibers is not a necessary condition of wetting the microfiber network.

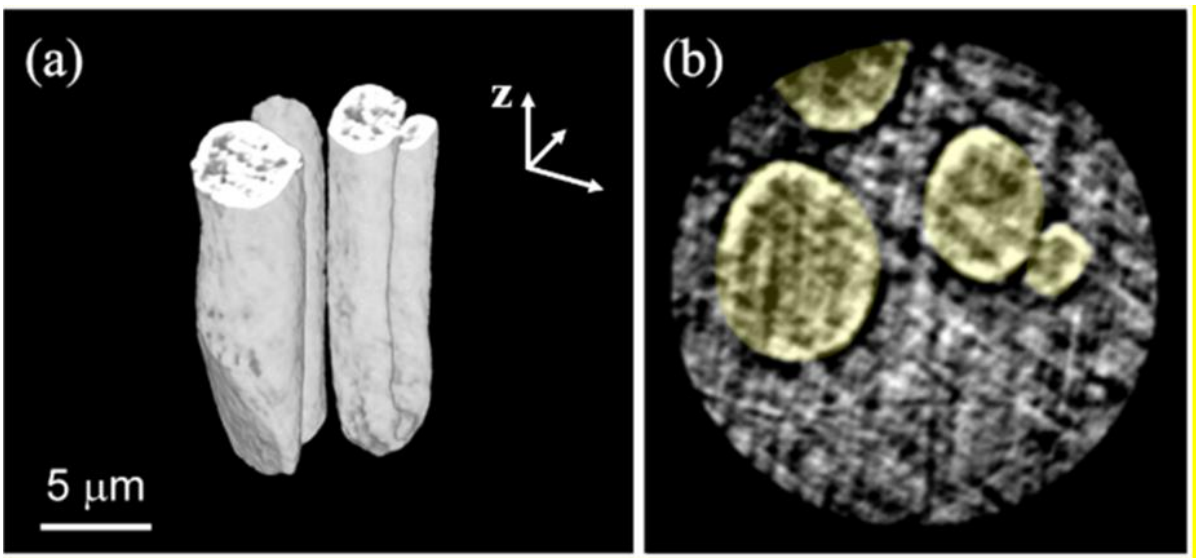

Figure 2.1. 3D transmission x-ray microscopy (TXM) image (a) and cross-section (b) of several 3M 8210 N95 respirator microfibers. The microfibers appear to have some surface roughness and porosity. Image reproduced with permission from Lam et al. [8].

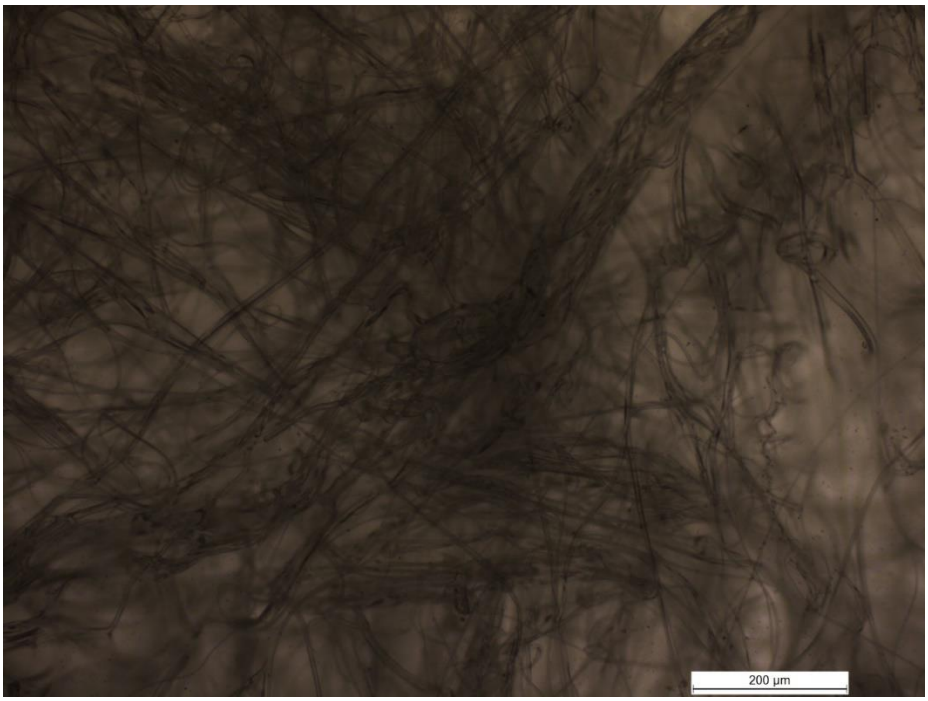

Figure 2.2. Light microscope image of the polypropylene microfiber electret filter of a 3M 8210 N95 respirator. Image was made with a Leica DM2500 P microscope with a Leica DFC290 HD digital camera. The scale bar in the lower right corner represents 200 μm.

2.2 Wetting of a Smooth Microfiber

Through the Young equation (eq. 2.1), we can relate the surface tensions of the three phases of a droplet/substrate system (solid-vapor, solid-liquid, and liquid-vapor), to the contact angle the liquid makes with the surface of the substrate.

$$\frac{\gamma_{SV}-\gamma_{SL}}{\gamma_{LV}} = \cos\theta \qquad (2.1)$$

The $\gamma_{SV} - \gamma_{SL}$ term can be determined experimentally for a solid and is known as the surface free energy (SFE). The SFE is important as it determines the critical liquid-vapor surface tension below which a liquid will wet the solid with the given SFE (eq. 2.2).

$$\gamma_c = (\gamma_{SV} - \gamma_{SL}) \qquad (2.2)$$

For certain materials, like most metals, the SFE is quite high (pure aluminum has a SFE of 1140 mN/m) [20]. As a result, these materials have associated critical surface tensions above that of any known liquid (mercury has a surface tension of 435 mN/m) [21]. These materials with sufficiently "high energy" surfaces are wetted by all liquids.

Equation 2.2 is more interesting for so called "low energy" surfaces, like those of many polymers, where the SFE, and thus the critical surface tension, is below that of water (~72 mN/m) [13]. For bulk polypropylene, a widely used polymer in electret filters, the SFE has been reported as 29.0-36.6 mN/m [22][23]. This relatively low SFE means that polypropylene is not wetted by pure water or by many aqueous solutions. Only liquids with a surface tension below ~30 mN/m, like ethanol (22.3 mN/m) and acetone (23.0 mN/m), can wet smooth polypropylene [13][14].

2.3 Wetting of a Rough Microfiber

The wetting transition as described by equation 2.2 is only valid for smooth surfaces. The impact of surface roughness on the wettability of a polymer surface can be understood through the Cassie-Baxter model (eq. 2.3) [24].

$$\gamma_{LV}\cos\theta^* = \sum_{i=1}^{n}\varphi_i\left(\gamma_{i,SV} - \gamma_{i,SL}\right) \qquad (2.3)$$

In equation 2.3, γ_{LV} is the surface tension of the applied liquid, θ^* is the apparent contact angle, and φ_i is the fraction of a solid's surface having surface energy $\gamma_{i,SV} - \gamma_{i,SL}$. For rough polypropylene, the second surface is air, and the result is:

$$\gamma_{LV}\cos\theta^* = \varphi(\gamma_{SV} - \gamma_{SL}) - (1-\varphi)\gamma_{LV} \qquad (2.4)$$

When the air fraction goes to zero ($\varphi \to 1$), equation 2.1 is recovered. Full wetting occurs in this model when θ^* approaches zero. The following relationship for the critical surface tension and the surface roughness is then found:

$$\gamma_c = \frac{\varphi(\gamma_{SV}-\gamma_{SL})}{2-\varphi} \qquad (2.5)$$

As a polymer surface gets rougher (φ decreases), the critical surface tension for wetting decreases. When a liquid's interaction with a solid is described by equation 2.4, the liquid is in a Cassie-Baxter state. A requirement for the Cassie-Baxter state is that the liquid's surface tension be above the critical surface tension described in equation 2.5. If the liquid's surface tension is below this critical value, the liquid will be in the fully wetted Wenzel state. A visualization of the Cassie-Baxter and Wenzel states was generated through the Surface Evolver software (Fig. 2.3) [25].

An important assumption in the Cassie-Baxter model is that the roughness of a surface is reasonably regular. For an individual microfiber, the surface is likely regular enough to be properly described by the model. In the hypothetical case of a mildly rough ($\varphi = 0.9$) polypropylene microfiber (and assuming a SFE of 32.5 mN/m), equation 2.5 predicts a critical surface tension of 26.6 mN/m, a reduction of almost 6 mN/m from the SFE.

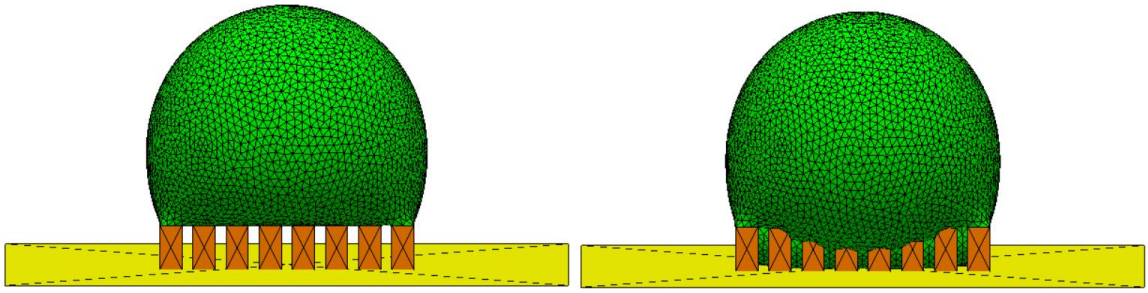

Figure 2.3. The Cassie-Baxter state (left, $\gamma_{LV} > \gamma_c$) and The Wenzel State (right, $\gamma_{LV} < \gamma_c$) modeled using the Surface Evolver software. In this simulation, a droplet sits on a 3 by 8 square pillar array.

2.4 Wetting of Nonwoven Fiber Network

It is not clear how to apply the Cassie-Baxter model equations to the 100-micron scale wetting of a typical polymer microfiber electret filter due to the nonwoven nature of the typical filter (Fig. 2.2 and Fig. 2.4).

The system we want to analyze using equation 2.6 is the dewetting of an array of microfibers (Fig. 2.5a). To simplify this system, we will first consider dewetting in the vicinity of a single, smooth fiber by comparing the free energies of a surface wetted state (Fig. 2.5c) to a vapor-boundary state (Fig. 2.5d). In equations 2.7 and 2.8, the free energy of the surface wetted state (F_W) and of the vapor-boundary state (F_{VB}) are given in terms of the three interfacial tensions ($\gamma_{SV}, \gamma_{SL}, \gamma_{LV}$), the area of the liquid-vapor interface (A_{LV}) and the surface area of the microfiber (A_S).

$$F_W = \gamma_{SL} A_S \qquad (2.7)$$

$$F_{VB} = \gamma_{SV} A_S + \gamma_{LV} A_{LV} \qquad (2.8)$$

$$F_{dry} = \gamma_{SV} A_S \qquad (2.9)$$

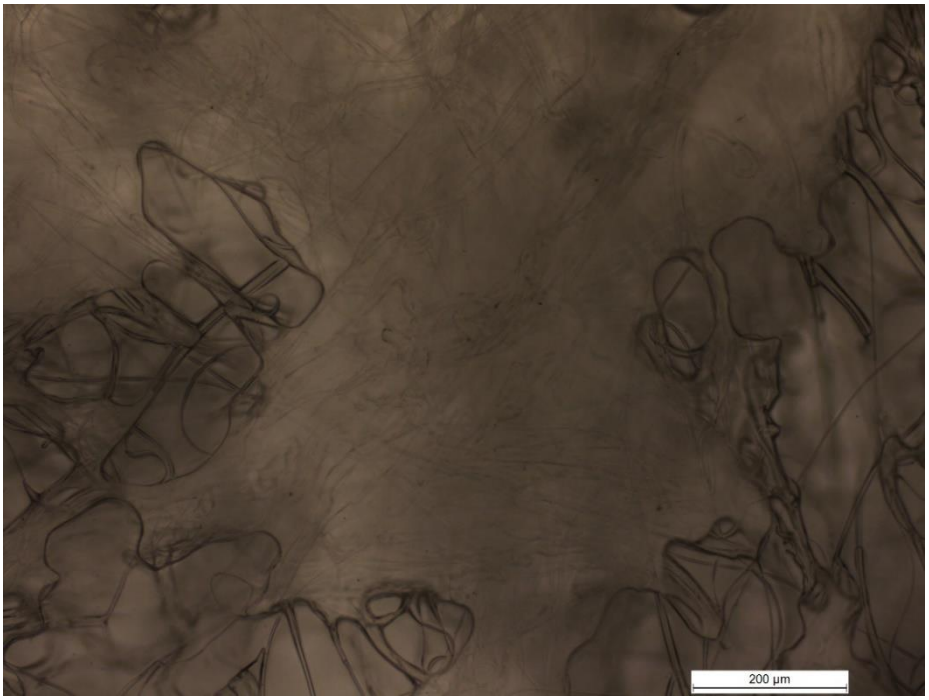

Figure 2.4. A 3M 8210 N95 respirator filter sample, wetted with 100% ethanol, in the process of dewetting. The filter sample was the same as in Fig. 2.2. Image was made with a Leica DM2500 P microscope with a Leica DFC290 HD digital camera. The scale bar in the lower right corner represents 200 μm.

The free energy of the completely dry fiber (eq. 2.9) can be subtracted from equations 2.7 and 2.8 to give equations 2.10 and 2.11. The Young equation (eq. 2.1) can then be substituted into equation 2.10 to relate the free energy of the surface wetted state to the contact angle a droplet would make on the material.

$$\Delta F_W = (\gamma_{SL} - \gamma_{SV})A_S = -\gamma_{LV} A_S \cos\theta \qquad (2.10)$$

$$\Delta F_{VB} = \gamma_{LV} A_{LV} \qquad (2.11)$$

There is a physical constraint on A_{LV} in the vapor-boundary state (in eq. 2.11): A_{LV} must be larger or equal to A_S, the surface area of a microfiber, for a convex microfiber. This implies that $\Delta F_{VB} > \Delta F_W$ for any contact angle $\theta \in [0°, 180°)$ and surface tension γ_{LV}. Thus, once a single fiber is wetted, the wetted state will be energetically favorable independent of the liquid's surface tension or the contact angle the liquid makes with the fiber. Furthermore, the growth of any liquid-vapor interface from the surface of the fiber is energetically unfavorable (eq. 2.11).

The free energy for the entire microfiber array can be found by summing over all the fibers. For the case when all the fibers are wetted, the free energy of the array (F_{WA}) is given by equation 2.12 for N fibers with A_{S_i} the surface area of the ith fiber.

$$F_{WA} = \sum_{i=1}^{N} -\gamma_{LV} A_{S_i} \cos\theta \qquad (2.12)$$

$$F_{DWA} = \gamma_{LV} A_{Sample} \qquad (2.13)$$

If $\theta > 90°$, the F_{WA} state is metastable and a more stable liquid-array state can occur. This state, F_{DWA}, happens when the area of the liquid-vapor interface is A_{Sample}, the surface area outside the fiber array (eq. 2.13, Fig. 2.5b). Importantly, F_{DWA} is more stable than F_{WA} when the sample is large enough as F_{WA} scales with the sample's volume while F_{DWA} scales with the sample's surface area.

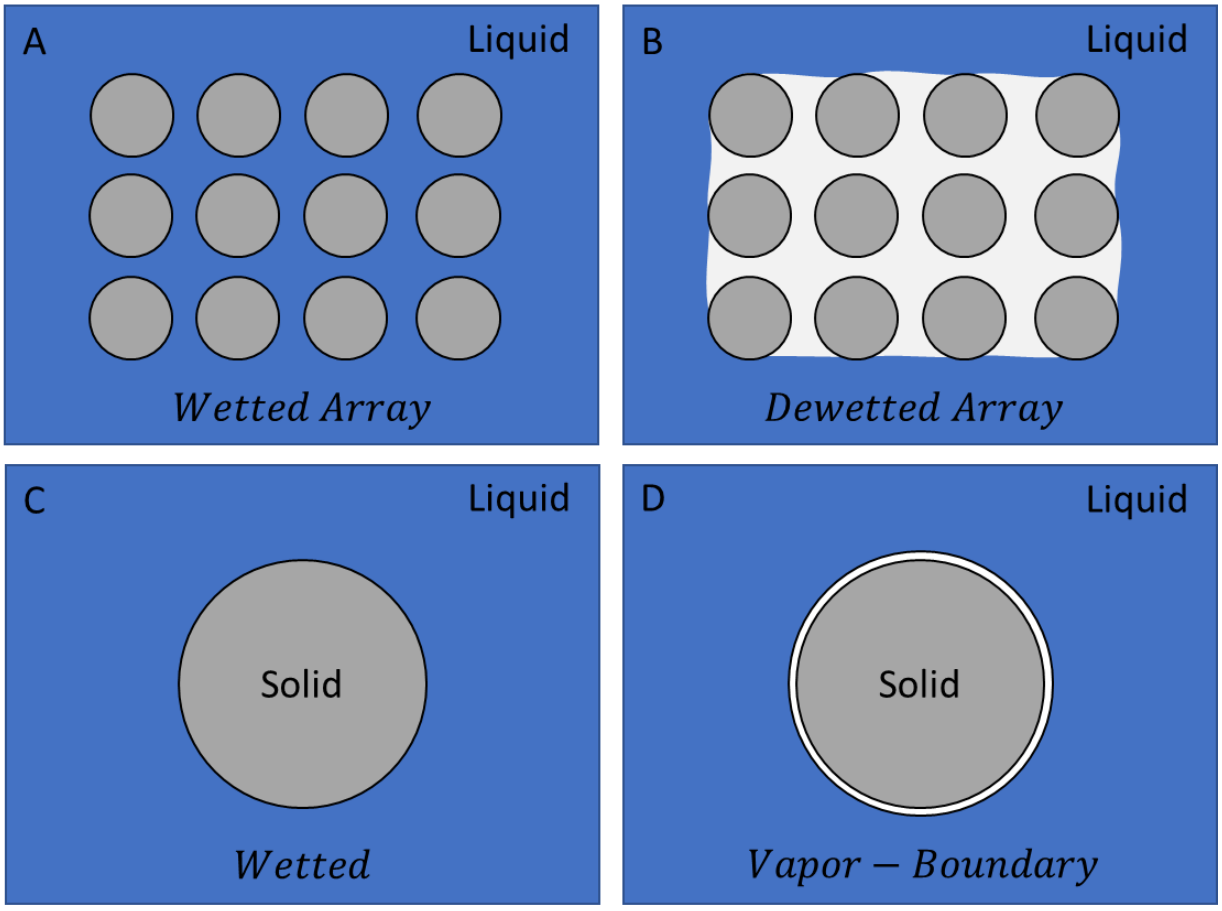

Figure 2.5. Illustration of various possible wetting states for an ordered fiber array (A and B) and a single fiber (C and D). (A) A wetted array is stable when the fibers are hydrophilic ($\theta < 90°$) and metastable (for large arrays) when the fibers are hydrophobic ($\theta > 90°$). (B) A dry array with a liquid-vapor interface at the surface of the array is stable (for large arrays) given the fibers are hydrophobic. (C) A single fiber immersed in solution is wetted for all contact angles except $\theta = 180°$. (D) An immersed single fiber can have a vapor-boundary layer only when $\theta = 180°$.

2.5 Predictions of Liquid-Induced Discharge from Wetting Theory

The liquid-induced discharge of a polymer microfiber electret filter should be dependent on the location of the solid-liquid interface. This location is itself dictated by the SFE of the polymer and the surface tension of the liquid and should be either: resting on outer fibers of the filter sample (Fig. 2.5b), on the surface of all the fibers (fig 2.5a), or, given a sample with rough and porous fibers, on and inside all the fibers (the Wenzel state). These possible locations for the

solid-liquid interface should occur, for a given polymer, sequentially as the surface tension of the liquid is decreased. The transition between the first and second solid-liquid interface locations (dry → wet array) should occur when $\gamma_{LV} = SFE$, but this transition can be forced when $\gamma_{LV} > SFE$ as the wetted array state is metastable even when the fibers are hydrophobic. The transition between the second and third solid-liquid interface locations (surface wetted → fiber penetration) should occur when the surface tension is below the critical surface tension (γ_c) given by equation 2.5.

For each of these solid-liquid interface locations, there should be a corresponding electret state in the filter: "undisturbed," "partially discharged," or "fully discharged." When the interface is outside the filter, very few fibers can be discharged resulting the "undisturbed" state. When the interface is resting on the surfaces of all the microfibers, the first trap layer near the fiber surfaces is discharged resulting in the "partially discharged" stated. Finally, if the liquid has penetrated the microfibers, most, if not all, the trapping sites are accessible to the liquid resulting in the "fully discharged" state.

Chapter III: Wetting Experiments

This chapter examines the wetting of polypropylene electret filters (taken from 3M 8210 N95 respirators) with ethanol/water solutions. The relevant physical properties of these solutions are discussed, and parts of the wetting theory developed in the previous chapter are confirmed qualitatively.

3.1 Liquid Treatment Methods

Solutions of various weight per weight (w/w) concentrations of ethanol (200 proof, VWR) and lab deionized (DI) water were prepared. The specific solution concentrations were chosen to match the concentrations used by Vazquez et al., as the surface tension of each ethanol/water solution could be inferred from their data [13].

Table 3.1. Surface Tension of Ethanol/Water Solutions at 20˚C

Solution EtOH % (w/w)	Surface Tension mN/m
0	72.75
5	56.41
10	48.14
15	42.72
20	38.56
25	36.09
30	33.53
40	30.69
50	28.51
60	26.72
70	25.48
80	24.32
90	23.23
100	22.31

Data from Vazquez et al. [13]

An important, but not unique trait to ethanol/water solutions is that below the azeotropic concentration (95.8% EtOH w/w) [27], the mole fraction of ethanol in the solution's vapor is greater than the mole fraction of water in the vapor (Fig. 3.1). As the surface tension of an ethanol/water solution strictly increases with decreasing ethanol concentration (table 3.1), an ethanol/water solution (with concentration <95.8% EtOH w/w) will see its surface tension increase as the solution evaporates away. Thus, if a filter is treated with an ethanol/water solution with a concentration below the azeotrope, the minimum surface tension the filter will be subjected to is the initial surface tension of the solution. This phenomena is not relevant to the wetting experiments in this chapter, but it is important to the thermally stimulated discharge (TSD) and filtration experiments.

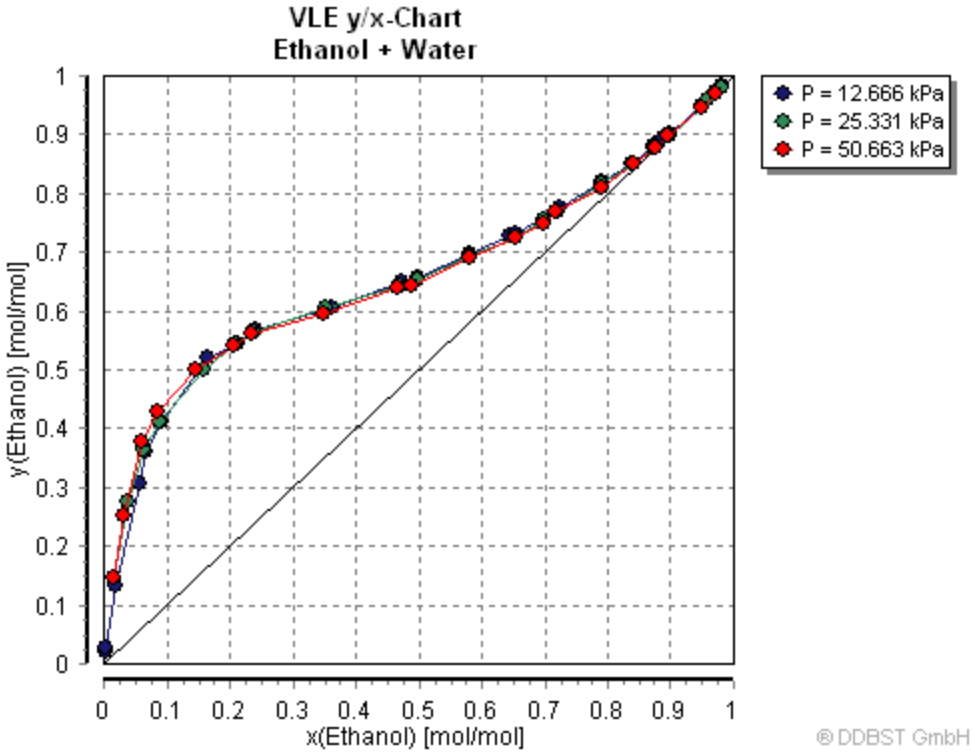

Figure 3.1. Vapor-Liquid equilibrium data for ethanol/water solutions at various pressures. Below the azeotropic concentration (mol fraction EtOH in solution, x=0.9), the solution vapor has more ethanol than water in it. Figure freely reprinted from the Dortmund Data Bank [28].

3.2 Wetting of Electret Filter Samples

Wetting experiments were conducted on polypropylene microfiber electret filter disks harvested from 3M 8210 N95 respirators. Liquid treatment consisted of placing a filter disk in a 100 ml beaker with approximately 20 ml of the selected liquid for an hour. Immersion of the filters was ensured by the weight of a pair of tweezers (Fig. 3.2).

When the concentration of ethanol was at or below 20% w/w, the liquid did not appear to wet the filter samples. At this concentration range a liquid-vapor interface was visible at the boundary of the filter samples and the samples were buoyant (Fig. 3.2a). Partial wetting of the sample was observed at 25% EtOH w/w and full wetting was seen at 30% EtOH w/w. At and above 30% EtOH w/w, the filter samples appeared to be fully wet: the liquid-vapor boundary layer was no longer visible and the samples appeared less buoyant (Fig. 3.2b).

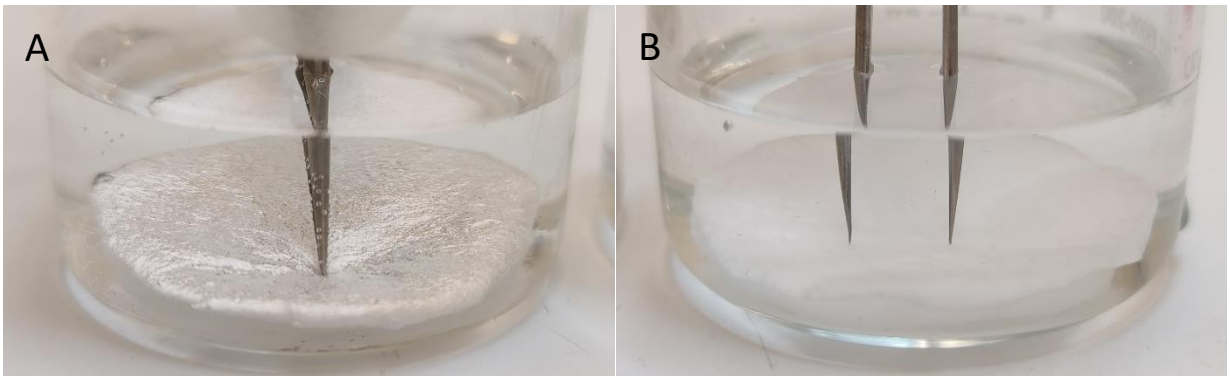

Figure 3.2. Wetting of polypropylene electret filters: (A) DI water. (B) 30% EtOH w/w. A prominent liquid-vapor interface is visible at the surface of the filter sample when immersed in DI water, but this interface is not present when the sample is immersed in a 30% EtOH w/w solution.

To better visualize the transition from dry to wet filters, ethanol/water solutions were prepared that had a 0.5 mM concentration of methylene blue dye. This specific dye concentration was chosen as it should be dilute enough to only modify the surface tensions of the ethanol/water solutions slightly [29]. The filters were then immersed in 20 ml of the various ethanol/water/dye solutions for an hour. To demonstrate the metastability of the wetted filter state, if the filter/liquid system did not spontaneously wet, a 3ml syringe was used to forcibly wet half the area of the sample (Fig. 3.3).

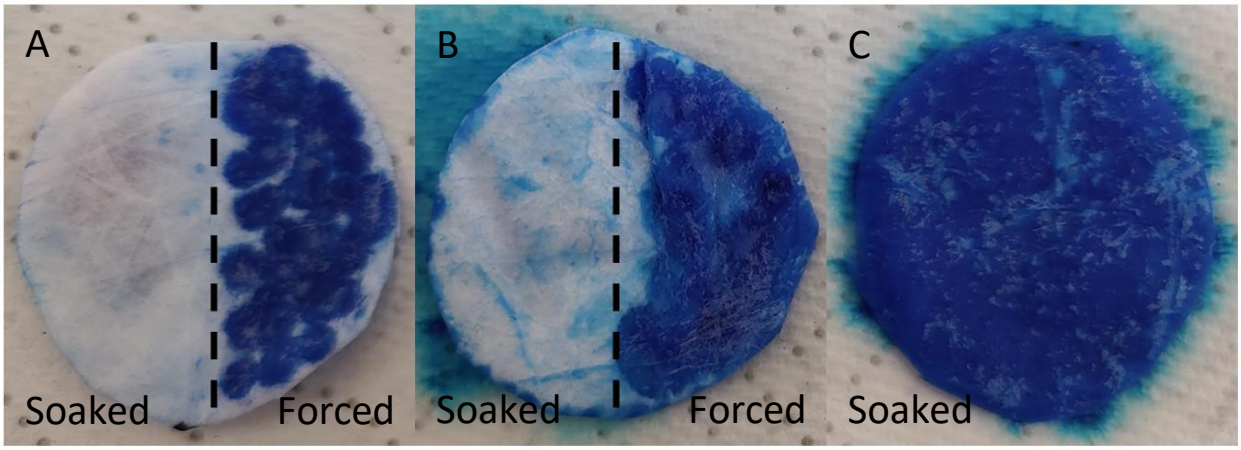

Figure 3.3. Wetting of polypropylene electret filters: (A) DI water. (B) 20% EtOH w/w. (C) 30% EtOH w/w. Each of these liquids had methylene blue dye added (at 0.5 mM concentration) to better visualize the wetting transition. In A and B, the filters were not spontaneously wetted by the 1-hour immersion ("soaked") in their respective liquid, so a wetted state was forced (via a syringe) on the right half of these samples (A and B).

3.3 Wetting Experiment Results and Discussion

A visible wetting transition occurred spontaneously in the samples when the ethanol/water solutions had a concentration around 25-30% EtOH w/w. This transition occurred

at approximately 33.5-36.1 mN/m, which is at the larger end of the literature reported values of the SFE of polypropylene.

As for the metastable wetted array state, this was observed when liquid was jetted with a syringe into filters that were not spontaneously wetted (Fig. 3.3). Qualitatively, the difficulty of obtaining this wetted state was proportional to the hydrophobicity of the system with the water/filter system markedly more difficult to wet than the 20% EtOH/filter system. However, in both cases once the wetted state was obtained, the state was long lasting (~hours, limited by evaporation).

Chapter IV: TSD Experiments

4.1 Thermally Stimulated Discharge of Electrets

An electret is an insulating material that holds a quasi-permanent electric charge distribution. Charges in electrets can be separated into several categories: surface charge, space charge, and polarization. These charge distributions create quasi-permanent electrostatic fields, which has resulted in the analogy of electrets as the electrostatic analog of magnets [4]. A powerful technique for studying these materials is thermally stimulated discharge (TSD) [30]. Generally, the technique entails sandwiching an electret between two electrodes and measuring the current generated by the sample as it is heated up. The resulting TSD current gives information on the electrical structure of the electret.

There are many variations on the TSD technique, but two distinctions relevant for this thesis are TSD experiments with measurement electrodes in a "shorted" or "open circuit" configuration (Fig. 4.1). The former only measures dipole relaxation in the sample, while the later can measure both dipole relaxation and charge neutralization [30]. A limitation of the "open circuit" TSD technique is the thickness of the sample, but as the polypropylene electret filters used in this work are ~350 μm thick when compressed, this is not an issue. All TSD experiments in this work were done in the "open circuit" configuration facilitated by using a 100 μm thick Teflon (PTFE) spacer in between the sample and one of the electrodes.

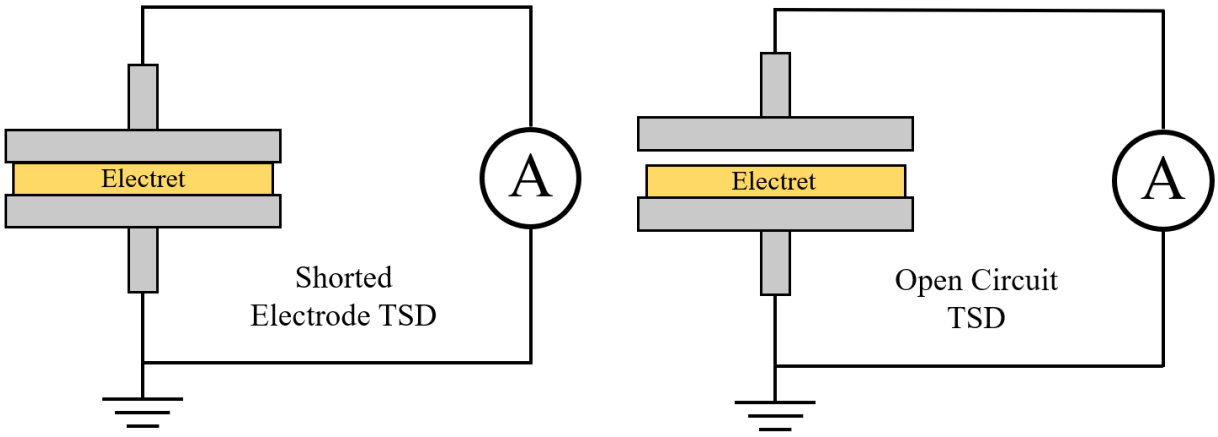

Figure 4.1. General schematic of "Shorted" and "Open Circuit" TSD experiment configurations. To run the experiment, the electrodes/electret were placed in an oven and heated at a constant rate.

4.2 TSD Theory

To obtain information on an electret's electrical structure, the current versus temperature data generated by a TSD experiment needs to be analyzed. Naïvely, one might think that this current data could be simply integrated to give an initial charge/polarization of the sample, but as there are several possible discharge mechanisms, this is not necessarily the case. Furthermore, competing discharge mechanisms can hide or partially cancel the effect of other mechanisms. A

simple example of this is an electret that has trapped an equal number of positive and negative charge carriers; if the two charges are released at the same temperature the current will be zero. Similarly, the closer in temperature the different carriers are released, the smaller the measured TSD currents will be. However, if the TSD current peaks generated by different discharge mechanisms are sufficiently far apart, a charge/polarization can be attributed to each mechanism via integration of the TSD current.

For the samples measured in this work, it was found that the largest TSD peak was dependent on the direction of the sample (Fig. 4.6). This suggests that the primary charge distribution in the samples was a polarization. To analyze this TSD peak, the single relaxation time dipole depolarization theory, as laid out in *Electrets*, was used [30].

This depolarization theory models an electret as containing numerous noninteracting dipoles, with the alignment of the dipoles resulting in a net polarization P_o. The electret is depolarized by increasing its temperature T at a linear rate, resulting in a TSD current density $i(T)$. If the dipole depolarization is the only discharge mechanism, the polarization of the sample can be calculated through equation 4.1, where h is the inverse heating rate dt/dT and T_o is the initial temperature of the sample. For a real electret, with multiple discharge mechanisms, the polarization can be calculated similarly as in equation 4.1, but the limits of integration need to only encompass the effect of the dipole peak in $i(T)$, if this is at all possible. Analysis of dipole polarization in this thesis used equation 4.2, where t_o and t_f are the times corresponding to the beginning and end of the dipole peak. This recasting exploits the fact that time and temperature are related through the linear heating of the sample. This approach also minimizes the effect variations in the heating rate have on the calculated net polarization.

$$P_o = h\int_{T_o}^{\infty} i(T)dT \qquad (4.1)$$

$$P_o = \int_{t_o}^{t_f} i(t)dt \qquad (4.2)$$

An important assumption in the depolarization theory laid out in *Electrets* is that all the dipoles have the same relaxation frequency $\alpha(T)$. Given this, the TSD current density generated by the depolarization is given by equation 4.3. The relaxation frequency $\alpha(T)$ is normally supposed to follow an Arrhenius equation (eq. 4.4) where α_o is the natural relaxation frequency of the dipole, A is the activation energy of the dipole trap, and k is the Boltzmann constant. Figure 4.2 shows a modeled TSD depolarization current using a set of parameters taken from Kravtsov et al. [1].

$$i(T) = -\alpha(T)P_o exp\left[-h\int_{T_o}^{T}\alpha(T)dT\right] \qquad (4.3)$$

$$\alpha(T) = \alpha_o exp\left[-A/_{kT}\right] \qquad (4.4)$$

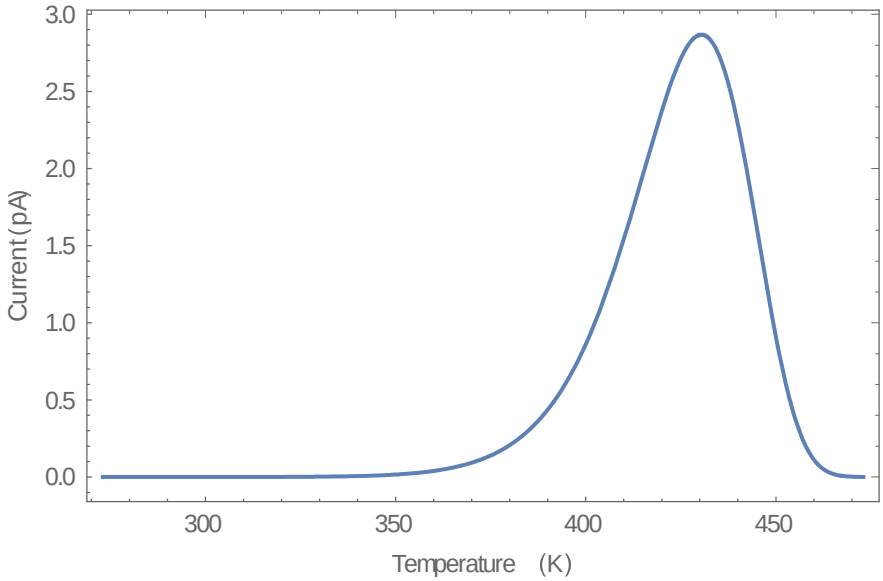

Figure 4.2. Modeled depolarization TSD current (through eq. 4.3, 4.4) for a $20 \times 20 \times 0.5$ mm electret with parameters: $P_o = 5\,\mu C/m^2$, $\alpha_o = 2 \cdot 10^9\ s^{-1}$, and $A = 0.99\ eV$. Plot was generated using Mathematica.

Using equations 4.3 and 4.4, the activation energy A of the dipole trap can be determined from the TSD data. During the initial rise of the TSD current peak, the integral term in equation 4.3 is small (eq. 4.5). By differentiating the logarithm of the current density (eq. 4.3) with respect to inverse temperature (in the initial rise regime), equation 4.6 is obtained [30]. This equation implies that the activation energy can be determined by a linear fit of the logarithm of the TSD current data plotted against inverse temperature (see Appendix A: TSD Data Analysis, Fig. A.2 for an example implementation).

$$h \int_{T_o}^{T} \alpha(T) dT \simeq 0 \qquad (4.5)$$

$$\frac{d}{d(1/T)} \ln i(T) = -A/k \qquad (4.6)$$

Another method of determining the activation energy A, is by measuring the full width at half maximum (FWHM) of the TSD current peak [30]. Equation 4.7 shows this approach with ΔT, the peak's FWHM, and T_m, the temperature corresponding to the maximum TSD current, related to the activation energy.

$$\Delta T / T_m \simeq 2.47 \cdot k \left(T_m / A \right) \qquad (4.7)$$

4.3 TSD Sample Preparation

Sections of 3M 8210 N95 respirators were cut into 35mm diameter disks. Each 35mm disk consisted of three parts: a polyester coverweb, a polypropylene electret filter, and a polyester shell (Fig. 4.3) [3]. As electrets can have a polarization, consistency in the orientation of the 35mm samples was important. Orientation was kept consistent in the sample preparation

phase by discarding the polyester coverweb and keeping the polypropylene electret filter and polyester shell together. The convention used in this project was to use the vector normal to the "outside" surface of the mask as the "up" direction of the polypropylene filters.

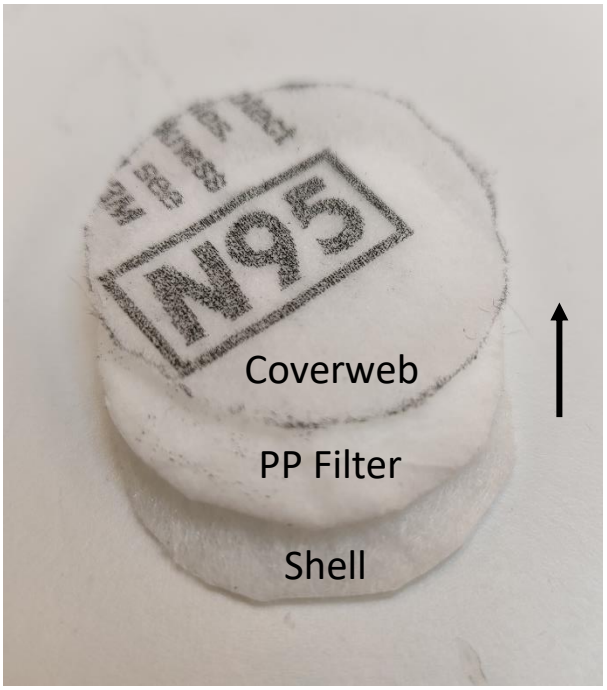

Figure 4.3. A 35mm sample disk cut from a 3M 8210 N95 respirator. The sample consists of 3 layers: a polyester coverweb, a polypropylene (PP) filter, and a polyester shell. The black arrow represents the "up" direction of the polypropylene electret filter.

Most of the filter samples were treated with ethanol/water solutions prior to being thermally discharged (see Ch. 3.1 for solution specifics). Liquid treatment consisted of placing a sample disk in a 100 ml beaker with approximately 20 ml of the selected liquid for an hour. Immersion of the samples was ensured by the weight of a pair of tweezers.

After an hour of immersion, the samples were removed from the beaker, placed on a paper towel, and allowed to air dry for 3+ hours. Once most of the liquid had evaporated, the samples were placed in a vacuum chamber and pumped on for 1 hour at ~1 mbar of pressure. The samples were then removed from the vacuum chamber and allowed to sit for another hour in the ambient laboratory conditions. This final step was important as the sample disks have enormous surface areas and some time is needed for the filters to equilibrate with the ambient humidity.

For filter samples which did not spontaneously wet (i.e., the EtOH treatment concentration was below 25% w/w), a sister sample was created. These sister samples were subject to the same liquid treatment protocols, but wetting was forced in the entirety of these samples using a 3ml syringe.

4.4 TSD Experiment Fabrication

A TSD apparatus was built by repurposing an ASC Scientific paleomagnetics demagnetization oven, fabricating a custom sample cell, and integrating the sample cell and oven with a Keithley 6487 picoammeter in LabVIEW.

The TSD sample cell (Fig. 4.4) was designed using van Turnhout's advice from *Electrets* [30]. The outer shield of the sample cell was machined by the author out of 303 Stainless Steel and the inner electrodes were machined out of 6013 Aluminum. The aluminum electrodes were stoned flat to ensure even pressure on the filter being tested. To isolate the electrodes from the outer shield, two 500 μm PTFE spacers were used. The electrodes were then connected to the picoammeter via a thermally insulated, low-noise triax cable. To reduce noise in the experiment, the negative electrode was guarded by electrically linking it to the outer shield. To control and measure the temperature of the sample cell, a type E thermocouple was thermally linked, but kept electrically isolated, to the sample cell via a beryllium oxide washer.

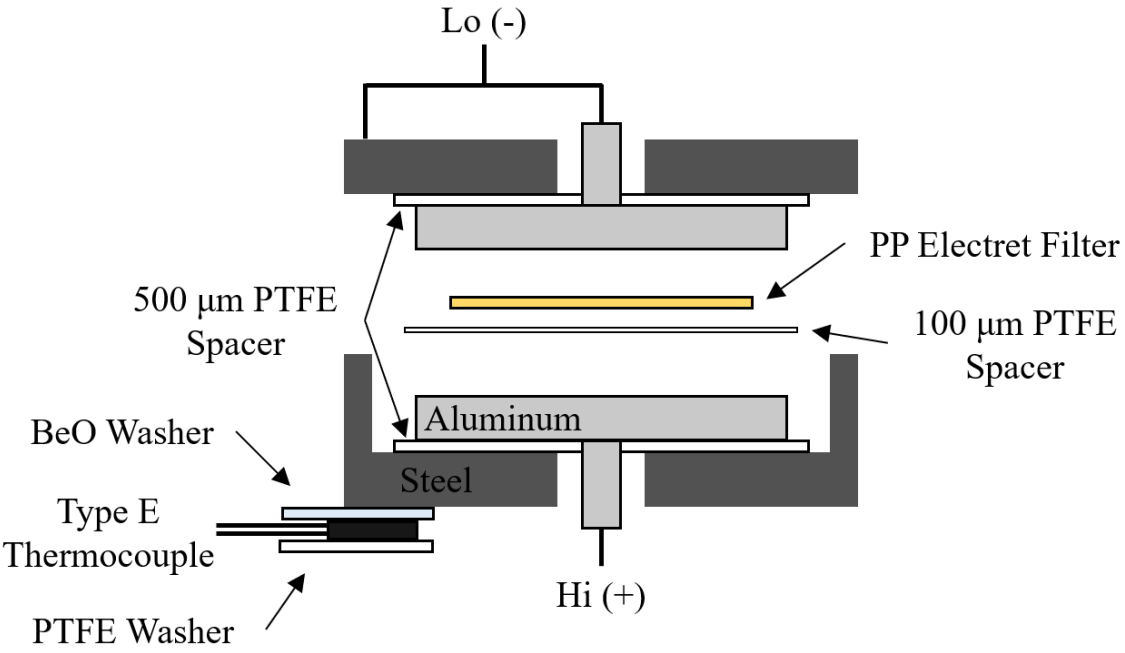

Figure 4.4. Exploded, cross-sectional view of the TSD sample cell. The normal orientation of the polypropylene (PP) electret filter was such that the "up" direction was towards the "Lo" electrode and away from the 100 μm PTFE spacer.

4.5 TSD Experiment Protocols

To run the experiment, the filter being tested was placed, along with a 100 μm PTFE spacer, in between the sample cell electrodes. The filter sample, electrodes, PTFE spacers, and outer shield were then sandwiched together, and the outer shield's lid was closed with six steel 4-40 screws. The 4-40 screws were driven in a star pattern by an electric drill (set to the 2nd lowest torque setting) to ensure an even and reproducible pressure on the filter being tested.

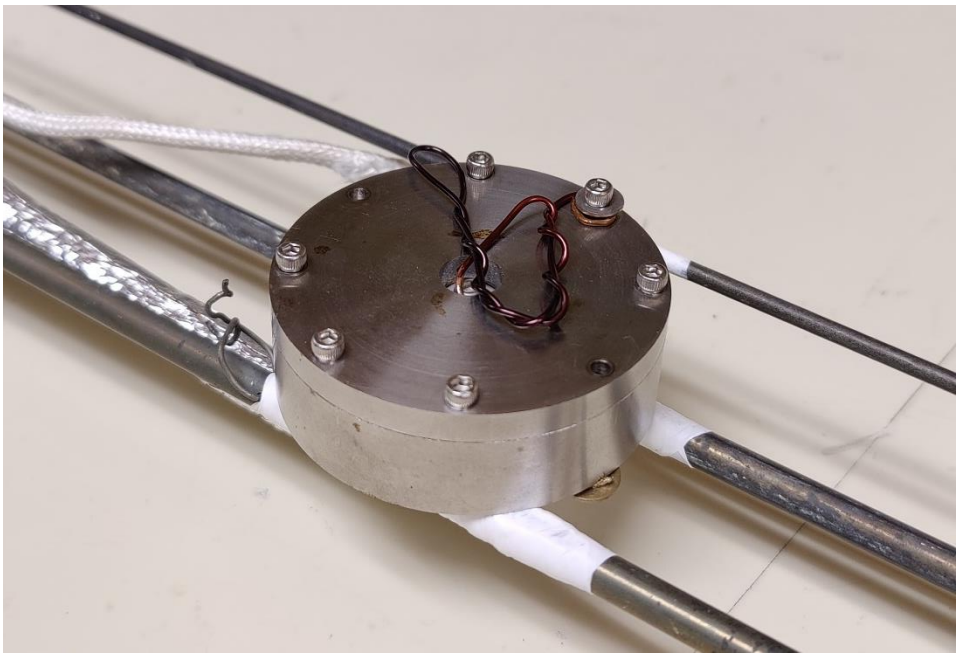

Figure 4.5. The TSD sample cell resting on a modified ASC Scientific oven insert.

The sample cell was then placed on an oven insert which had been wrapped with Teflon tape to electrically isolate the TSD sample cell from it (Fig. 4.5). The type E thermocouple was connected to the oven's CN76000 temperature controller and the sample cell's triax cable was connected to the Keithley 6487 picoammeter. The oven insert was then placed inside the (still room temperature) oven.

The sample cell was then heated at a constant rate from room temperature to $200℃$. Preliminary data was collected at a $5℃/min$ increase, but as the temperature resolution of different TSD peaks was insufficient at this rate, all data apart from Fig. 4.6 were collected at a rate of $2℃/min$. This relatively slow heating rate had the advantage of yielding better TSD peak resolutions with less temperature lag in the data, but it came at the cost of signal to noise ratio and required longer experimental run time.

Linear heating was achieved by programming the oven's CN76000 PID temperature controller to increase its set point temperature at a constant rate. For the first $\sim 10℃$ (from 25-35 Celsius) the heating was controlled manually as to match the derivative of the sample cell's temperature to the $2℃/min$ increase in the temperature controller's set point. This procedure minimized any integral windup and overshoot problems and resulted in a relatively linear heating of the sample cell (Fig. 4.7).

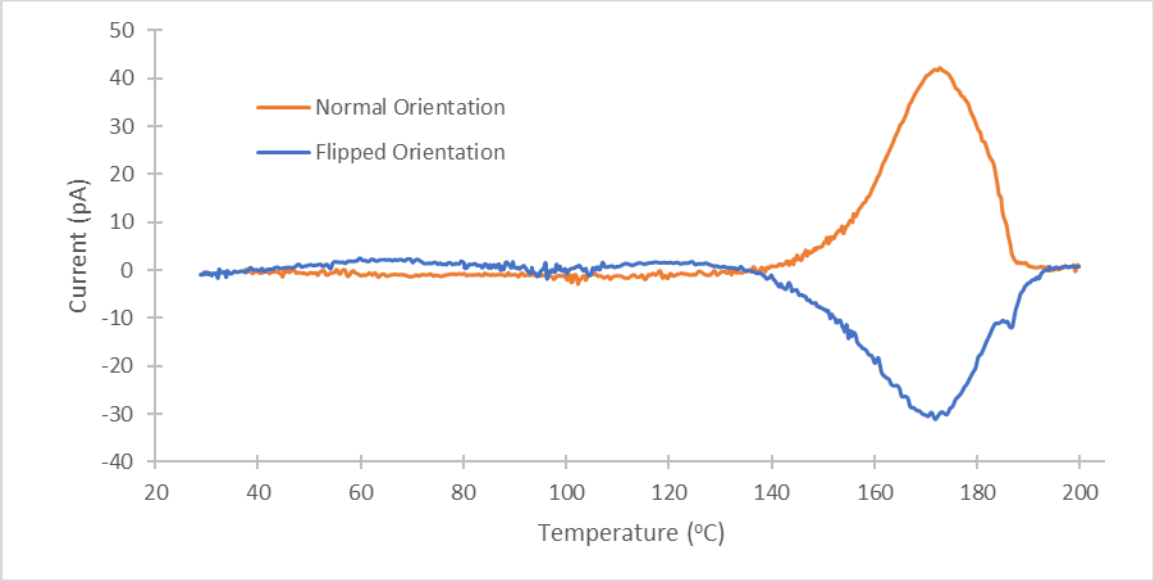

Figure 4.6. Preliminary TSD data showing the effect of sample orientation on the TSD current. The heating rate for this data was $5℃/min$. Notice the appearance of a partially hidden TSD peak at $\sim 185℃$.

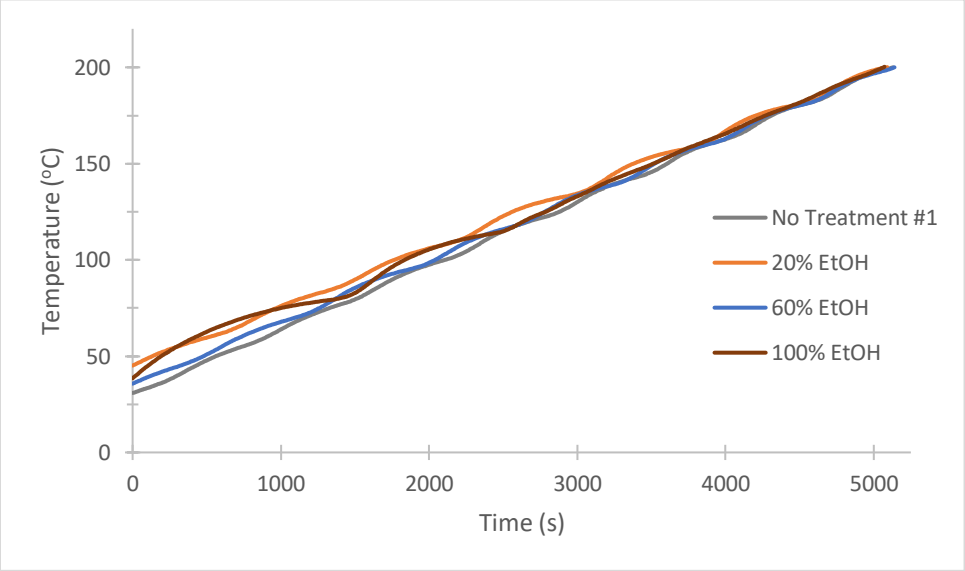

Figure 4.7. Sample cell temperature versus time for a few TSD runs. This plot shows the relative linearity achieved in the heating of the TSD samples.

Measurement of the sample cell's temperature and the thermally stimulated current was done in LabVIEW through modification of the Keithley 6487 and Omega CN76000 driver software. The default settings on the Keithley 6487 picoammeter were modified to improve the TSD data: the measurement time was extended from 6 to 10 power line cycles, a median filter of rank 3 was enabled, and a moving data average of 100 counts was enabled.

4.6 TSD Experiment Results and Discussion

TSD spectra were collected for untreated filter samples as well as samples soaked in DI water and various ethanol/water solutions (20%, 30%, 40%, 60%, 80%, 90% and 100% EtOH w/w). Additional TSD spectra were collected for samples that were forcibly wetted in DI water and 20% EtOH w/w. Fig. 4.8 shows the TSD spectra for two 35mm filter samples that underwent no liquid treatments and demonstrates the general capabilities of the TSD apparatus regarding reproducibility and peak resolution.

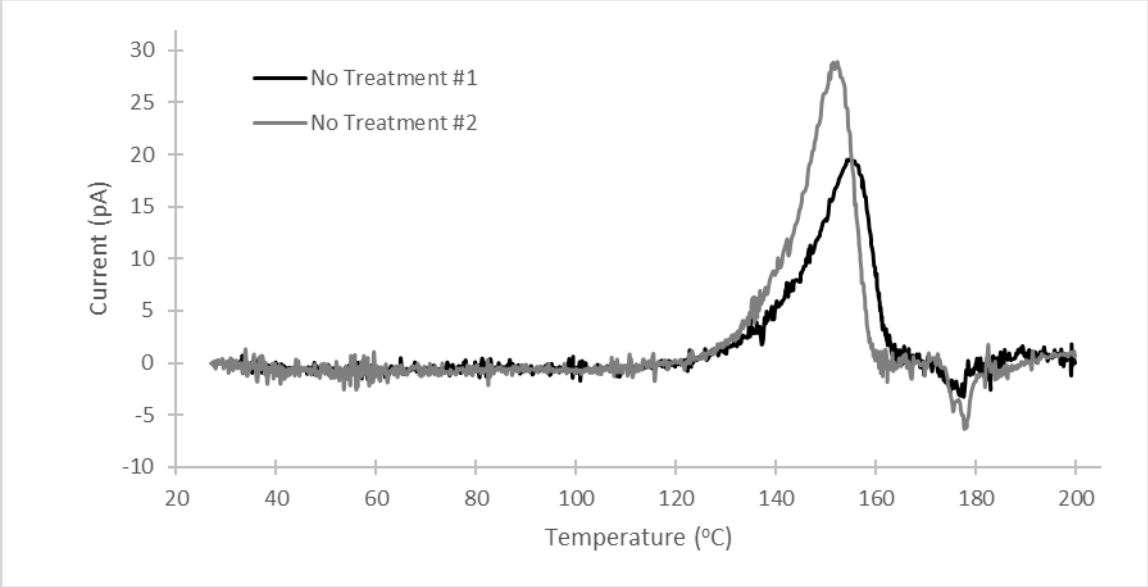

Figure 4.8. TSD current vs temperature for two untreated 35mm filter samples. There are two visible TSD peaks in each spectrum: a primary one at ~150℃ likely due to sample polarization and a secondary one at ~175℃ likely due to the release of charges inherent in polypropylene. Variations in the peak shape between the samples are explainable through nonlinearities in the heating (Fig. 4.9).

The ~150℃ TSD peaks seen in Fig. 4.8 appear to be resolved well enough to allow for a polarization to be calculated via equation 4.2. This peak resolution was achieved by using a $2℃/min$ heating rate and was critical in separating the ~150℃ peak from the ~175℃ peak (in contrast to Fig. 4.6). This situation is fortunate as the polarization calculation provides a method to quantitatively compare TSD spectra while minimizing the effect variations in the heating rate have on the results. For example, while the two TSD peaks look reasonably different in Fig. 4.8, the polarizations are within the experimental error at $9.14 \pm 1.23\,\mu C/m^2$ and $10.30 \pm 1.31\,\mu C/m^2$ for samples 1 and 2, respectively. Details on the TSD data analysis are available in Appendix A.

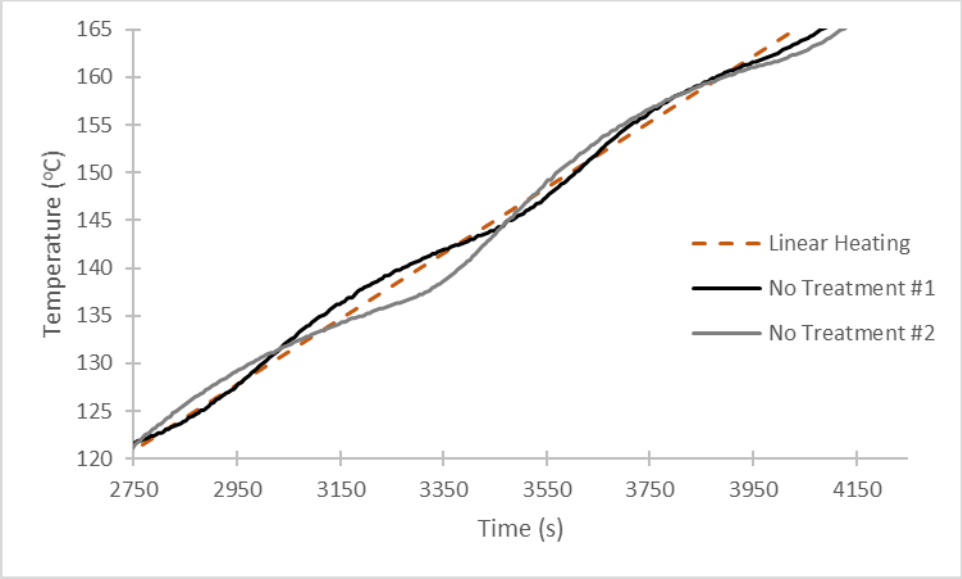

Fig. 4.9. TSD sample cell temperature versus time for the ~150℃ peaks in Fig. 4.8. A higher rate of heating increases a TSD peak's maximum current and correspondingly lowers the temperature at which this current maximum is achieved [30]. It appears that deviations in the heating rates for the two samples can explain the differences in peak shape seen in Fig. 4.8.

The TSD spectra collected in this thesis appeared to fall into one of three general categories: undisturbed, partially discharged, and fully discharged (Fig. 4.10 show representative samples of TSD spectra from these categories). These categories were defined by the shape of the ~150℃ TSD peaks and transitions from each category were related to the ethanol concentration of the treatment liquid. These transitions occurred sequentially with increasing ethanol concentration: the first transition was between 20-30% EtOH w/w and the second transition was between 90-100% EtOH w/w.

Liquid treatment appeared to only affect the ~150℃ peak, suggesting the ~175℃ peak originated from inherent charge in the polypropylene. This inherent charge hypothesis is further supported by the reported melting point of isotactic polypropylene fibers being between 164℃ and 177℃ with dependence on the crystallinity of the fibers [31]. Assuming this ~175℃ peak results from melting, and thus doesn't contribute to the electret effect at room temperature, then the 100% EtOH liquid treatment appears to have completely discharged the filter sample (Fig. 4.10).

The variations between several of the "partially discharged" TSD spectra can be seen in Fig. 4.11. The samples in this figure were all soaked in their respective ethanol/water solutions for an hour. Importantly, within the range of EtOH solutions corresponding to "partially discharged," (30-90% EtOH w/w) there did not appear to be a relationship between EtOH concentration and peak shape. This suggests that a single wetting regime, rather than an EtOH concentration effect, is responsible for this "partially discharged" electret state.

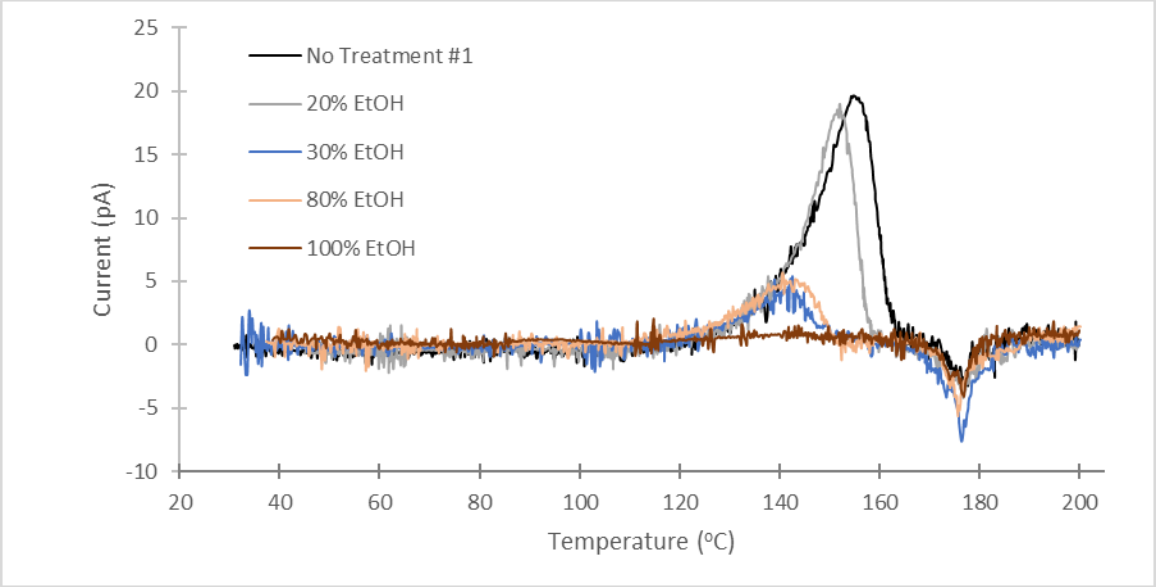

Fig. 4.10. A selection of TSD spectra showing the general outcomes of liquid treatment on the filter electret state. The spectra can be grouped into three general categories: undisturbed (No Treatment #1, 20% EtOH), partially discharged (30% EtOH, 90% EtOH) and fully discharged (100% EtOH). The ~175℃ TSD peak does not appear affected by the liquid treatments suggesting that this peak results from inherent charge in the polypropylene.

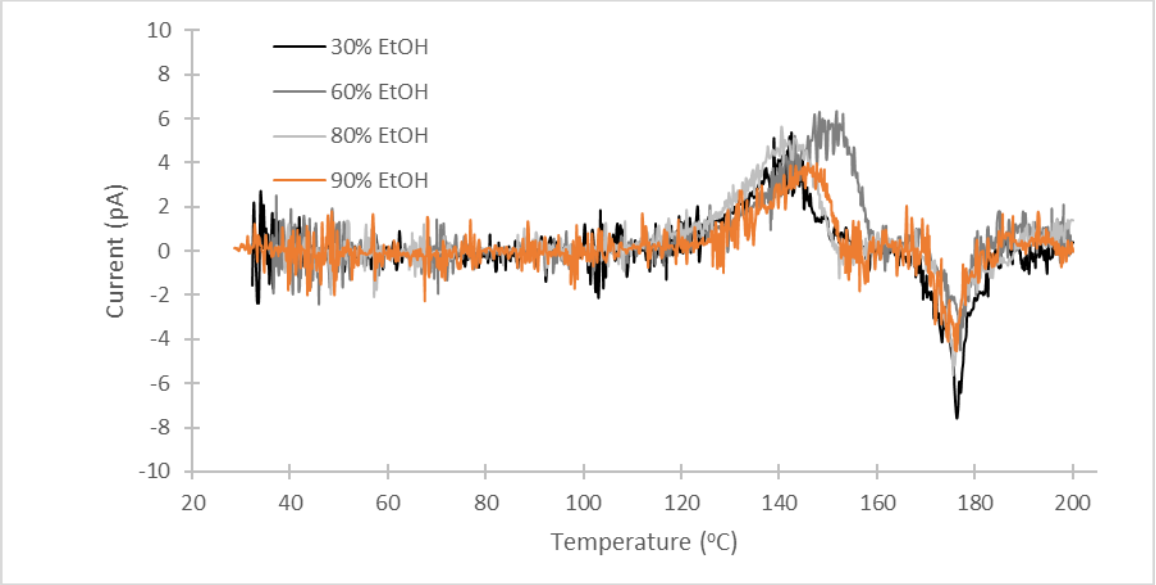

Figure 4.11. A selection of TSD spectra from the "partially discharged" regime. All these samples were soaked in their respective ethanol/water solutions for an hour. This "partially discharged" regime appears to span liquid treatments from 30-90% EtOH w/w.

As filter samples treated with DI water and 20% EtOH w/w did not appear to spontaneously wet (Fig. 3.3ab) sister samples for these concentrations were made where wetting was forced via a syringe. Figure 4.12 shows the resulting TSD spectra for these samples along

with two representative TSD spectra from the “partially discharged” classification seen in Fig. 4.10. The qualitative similarity between these spectra suggests that the forced wet samples should be included in the “partially discharged” classification. Furthermore, it seems likely that the “wetted array” wetting state (Fig. 2.5a) is the cause of the “partial discharge” filter electret state.

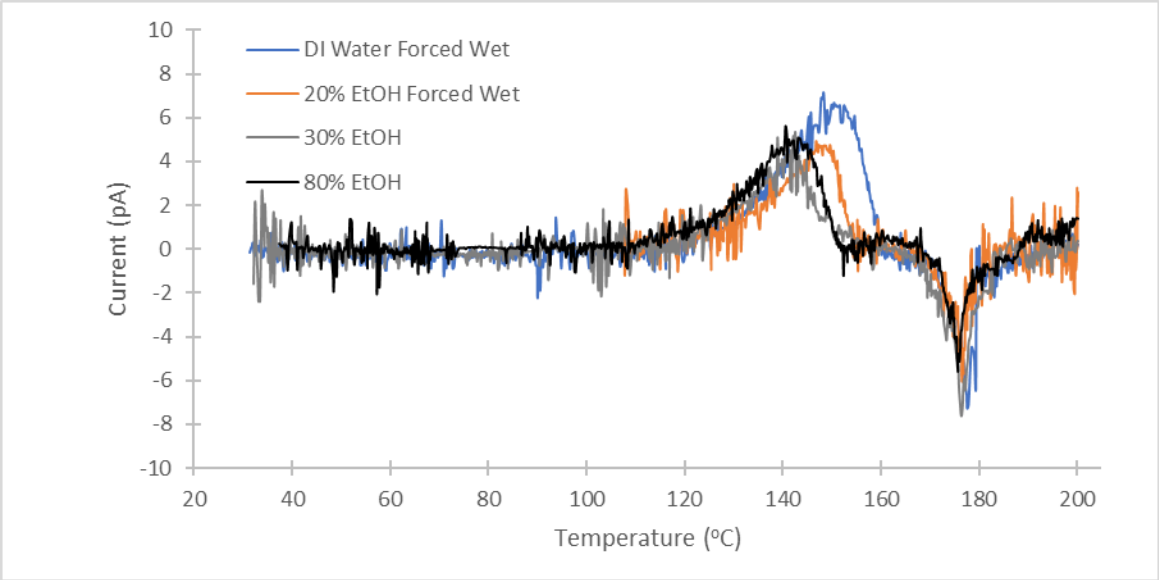

Figure 4.12. TSD spectra of the forced wet samples along with two representative TSD spectra from the “partially discharged” classification.

The classification of a TSD spectrum as “undisturbed,” “partially discharged,” or “fully discharged” is made more quantitative through the calculation of the polarization of the sample’s ~150℃ TSD peak. As the ~150℃ TSD peak holds the vast majority of a sample’s polarization, the polarization of this peak is referred to as the polarization of the filter in the remainder of this thesis.

The polarization of the filter versus the treatment liquid ethanol concentration is seen in Fig. 4.13. This figure supports the notion of three distinct electret filter states with the “undisturbed” state corresponding to the DI water and 20% EtOH w/w soaked filters, the “partially discharged” state corresponding to the forcibly wetted filters along with the filters soaked in 30-90% EtOH w/w, and finally the “fully discharged” state corresponding to the filter soaked in 100% EtOH.

Using the Vazquez et al. ethanol/water solution surface tension data (table 3.1), the filter polarization was recast against the surface tension of the treatment liquid (Fig. 4.14). As all the ethanol/water solutions, apart from 100% EtOH, were below the ethanol azeotrope, the surface tension of each treatment liquid corresponded to the minimum surface tension liquid applied to each filter. This recasting of the polarization data in terms of surface tension makes obvious the connection between the discharge theory developed in chapter 2 and this data.

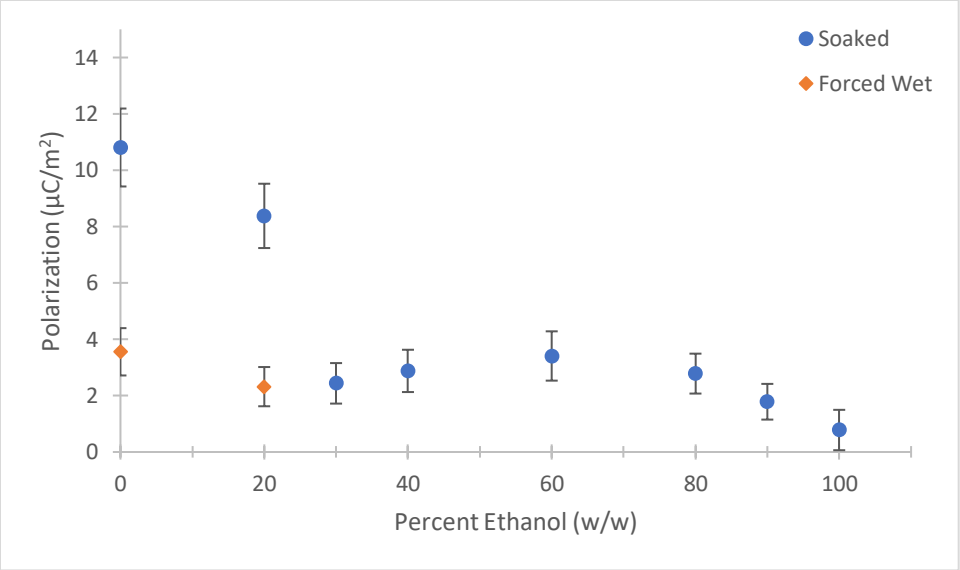

Figure 4.13 Filter polarization versus liquid treatment. Polarization of the untreated samples was $9.72 \pm 0.90\ \mu C/m^2$.

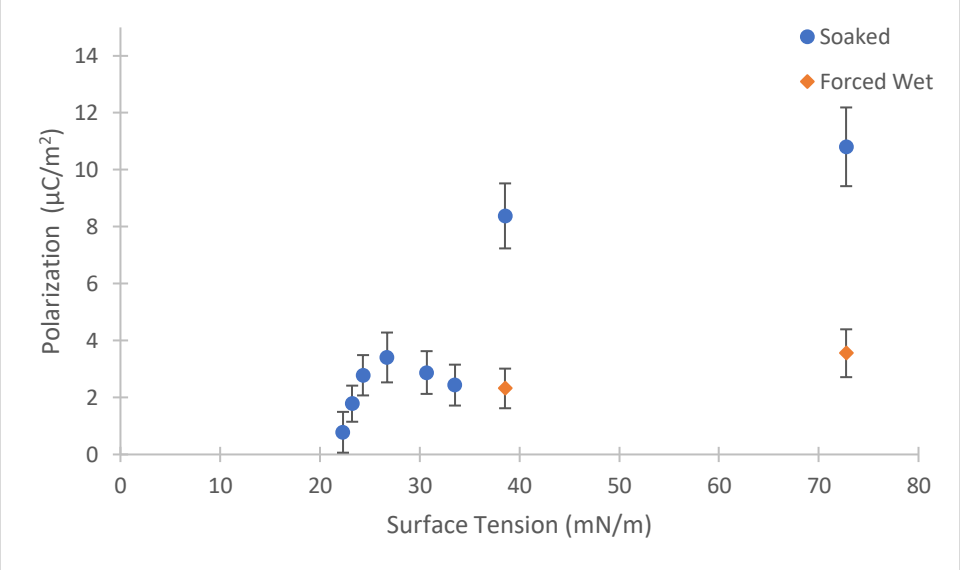

Figure 4.14. Filter polarization versus treatment solution surface tension. Polarization of the untreated samples was $9.72 \pm 0.90\ \mu C/m^2$.

When the filter was soaked in a solution with a surface tension above the SFE of polypropylene (reported between 29.0-36.6 mN/m), the solid-liquid interface rested on the outside of the filter (Fig. 3.2a) and the polarization appeared largely unaffected from its initial value. When the filter had been wetted (either spontaneously or forcibly), the solid-liquid interface rested on the outer surfaces of all the fibers, and the polarization appeared to drop to approximately 1/3 of its initial value. Finally, when the surface tension was low enough (below ~23.2 mN/m), the polarization dropped further, this time towards zero.

The transitions seen in Fig. 4.14 put bounds on the SFE of the filter and, through equation 2.5, put bounds on the roughness of the microfibers. The SFE is estimated as 33.5-38.6 mN/m and the roughness parameter φ is estimated as 0.73-0.82 from Fig. 4.14. The SFE estimate seems reasonable considering the literature reported values, and the roughness parameter (φ is 1 for a smooth surface) seems plausible given the structure of the individual microfibers (Fig. 4.15).

One of the hypotheses of chapter 2's discharge theory was that a liquid should only discharge the first layer of trapping sites near a solid-liquid interface. This hypothesis can be analyzed by calculating the depth discharged assuming the microfibers were initially uniformly polarized. Lam et al. measured the average microfiber diameter in a 3M 8210 N95 respirators as 2.9 μm, so given the "partially discharged" state removed approximately 2/3 of the initial polarization, the discharge depth is estimated as ~0.6 μm [8]. This calculation is somewhat questionable as the fibers are distributed in size, but it does appear to agree with the thickness of the polypropylene layer just below the surface of the microfibers as imaged by Lam et al. (Fig. 4.15b). This ~0.6 μm discharge depth also agrees with the expected size of spherulites in polypropylene microfibers (at or below 0.7 μm in diameter).

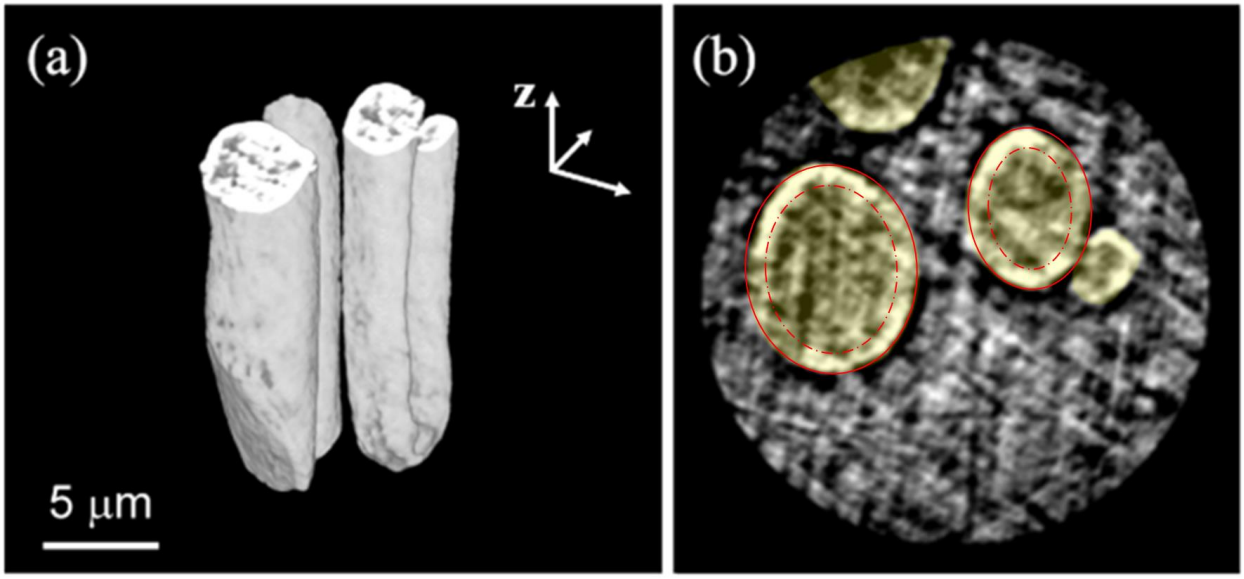

Figure 4.15. 3D transmission x-ray microscopy (TXM) image (a) and cross-section (b) of several 3M 8210 N95 respirator microfibers. The red lines overlaid on the fibers in (b) show the estimated 0.6 μm discharge depth. This discharge depth appears to correspond to the thickness of the polypropylene layer just below the surface of the microfibers. Image reproduced and modified with permission from Lam et al. [8].

The activation energies of the ~150℃ TSD peaks were calculated through both the FWHM method and the initial rise method for all the TSD spectra (see Appendix A: TSD Data Analysis for methods). Figure 4.16 shows the activation energies plotted against the treatment solution surface tension. The activation energies are the correct order of magnitude, but the variations in the values make it difficult to draw conclusions from the data. Both methods suggest that the activation energy decreases when the filter is wetted (i.e., $\gamma_{LV} < 38.6\, mN/m$, or

forced wet), but the methods appear to disagree on the size of the decrease. For the initial rise method, this discrepancy may be the result of fitting equation 4.6 to noise as a small TSD current peak has an even smaller initial rise. In any case, the inaccuracy in the activation energy calculations are not unexpected as the slow heating rate used in these TSD experiments was optimized for peak resolution and not signal to noise ratio.

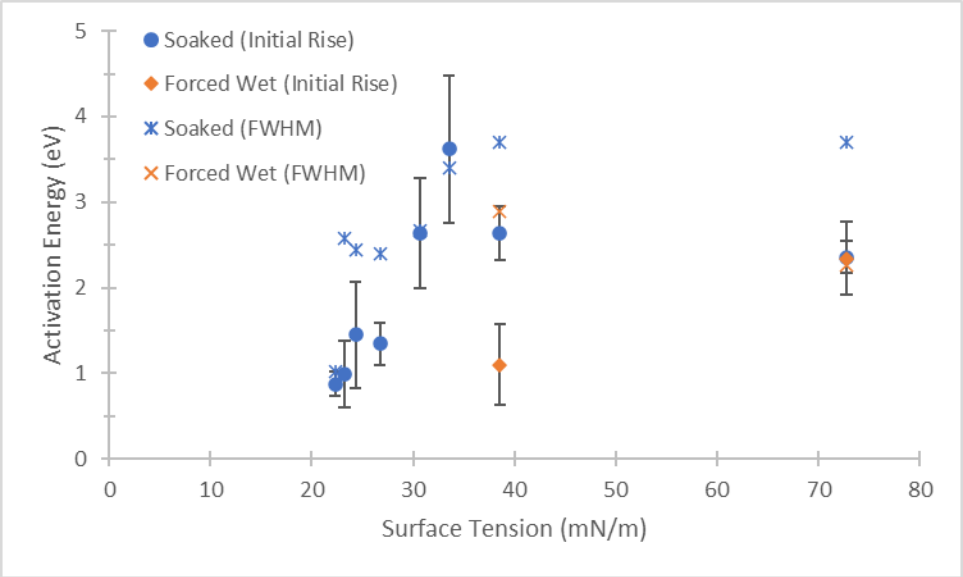

Figure 4.16. Dipole activation energy versus treatment solution surface tension. Activation energy was calculated through the initial rise method and the FWHM method.

Chapter V: Filtration Experiments

5.1 Respirator Liquid Treatment

Seven 3M 8210 N95 respirators were treated with various ethanol/water solutions (First trial: 10%, 62.4%, and 100% EtOH w/w; Second trial: 40%, 50%, 60% EtOH w/w). The 62.4% EtOH w/w solution was chosen as it corresponds to 70% EtOH v/v. Liquid treatment consisted of pouring ~50 ml of the selected liquid on the respirator. Once wet, the respirators were hung and allowed to air dry overnight for 8+ hours (Fig. 5.1). The respirators were then placed in a vacuum chamber and pumped on at ~1 mbar pressure for 4-6 hours. The respirators were removed from the vacuum chamber and allowed to equilibrate in the ambient laboratory conditions for 24+ hours prior to filtration measurements.

Figure 5.1. Three 3M 8210 N95 respirators air drying after liquid treatment.

5.2 Aerosol Penetration Measurement Methods

Aerosol penetration through the respirators was measured by Buddhi Pushpawela on the Flagan group's polydispersed NaCl aerosol filtration testing device. The device exposed the respirator-under-test to an electrically neutral NaCl particle aerosol and measured the aerosol particle size and concentration before and after the respirator (Fig. 5.2). The data collected by the device was displayed as an aerosol penetration versus aerosol particle size. Aerosol size was determined by a Long Differential Mobility Analyzer (LDMA) and aerosol concentration was determined by a condensation particle counter. The pressure drop across the respirator was also recorded and the flow rate of air through the respirator-under-test was set at 30 lpm.

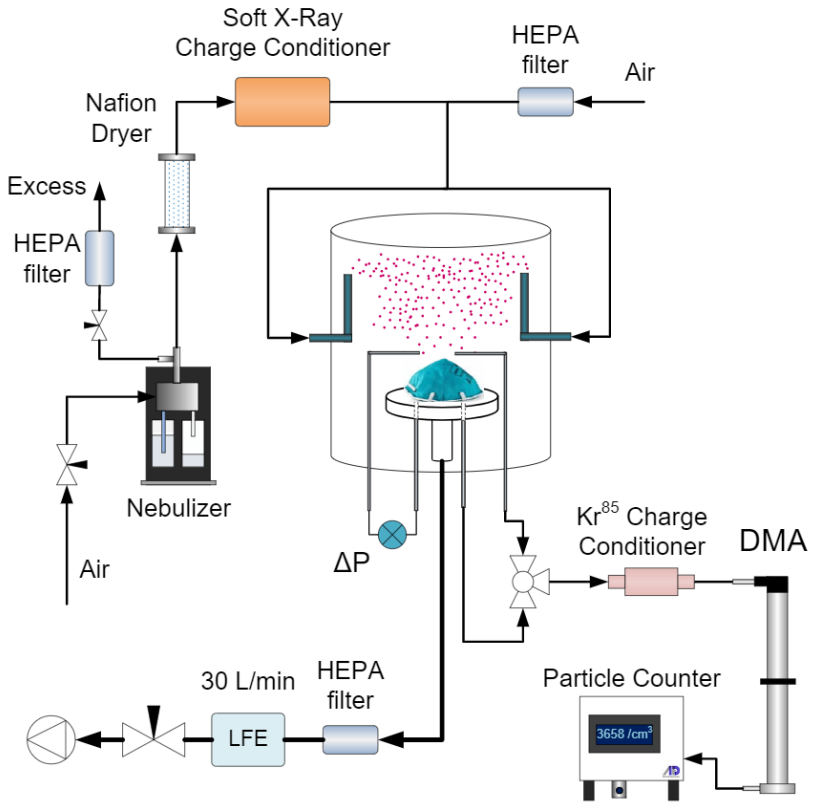

Figure 5.2. Polydispersed NaCl aerosol filter testing setup. Figure courtesy of Buddhi Pushpawela and the Flagan group.

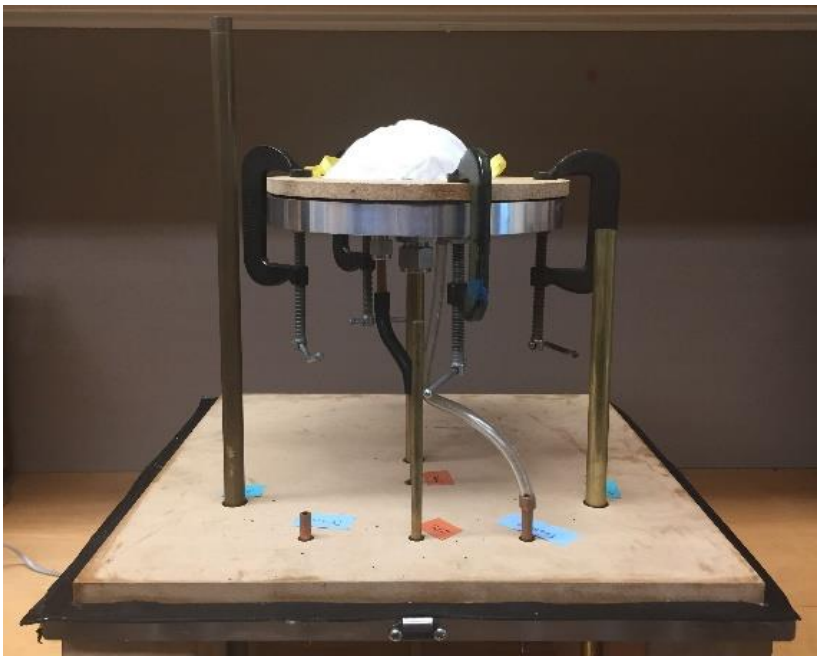

Figure 5.3 A 3M 8210 N95 respirator in the filtration testing device holder. The respirator was sealed by clamping it between a wooden plate with a central cut-out and a metal plate. Image courtesy of Buddhi Pushpawela and the Flagan group.

5.3 Results and Discussion

The aerosol penetration data shown in this thesis is preliminary and the Flagan group is continuing to improve their experimental techniques and data analysis methods. As the methods changed between the first trial (10%, 62.4% and 100%) and the second trial (40%, 50%, and 60% EtOH w/w) the data is displayed on two separate figures (Fig. 5.4 and Fig. 5.5). The observed decrease in the filtration efficiency of these filters in the 50 to 500 nm particle diameter regime supports the notion that increasing the ethanol treatment concentration decreases the electrostatic collection mechanism in the respirators [2]. Figure 5.4 suggests that there are three distinct electrostatic collection states, corresponding to the "undisturbed," "partially discharged," and "fully discharged" electret states seen in chapter 4. Importantly, the liquid treatment methods of this chapter involved pouring the treatment solutions on the respirators, implying that the filtration data should be compared to the "soaked" TSD and polarization results (Fig. 4.10 and Fig. 4.13). More specifically, the 10% EtOH w/w solution should result in the "undisturbed" filter electret state, the 62.4% EtOH w/w solutions should result in the "partially discharged" filter electret state, and 100% EtOH solution should result in the "fully discharged" electret filter state.

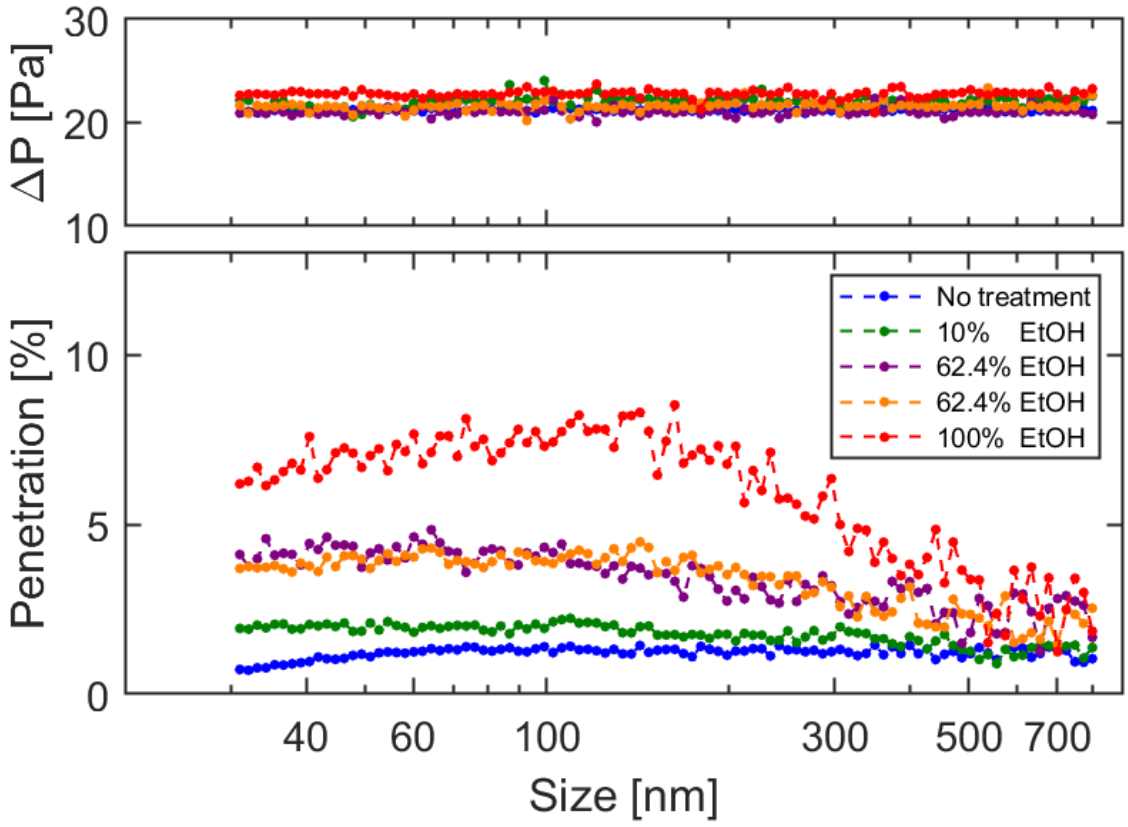

Figure 5.4. Penetration vs aerosol particle diameter for different liquid treatments of 3M 8210 N95 respirators. Figure courtesy of Buddhi Pushpawela and the Flagan group.

The finding in chapter 4 that a large range of ethanol concentrations (30-90% EtOH w/w) resulted in the same filter polarization is reflected in the filtration data in Fig. 5.5. This plot shows similar filtration performances for filters treated with ethanol concentrations from 40-60% EtOH w/w.

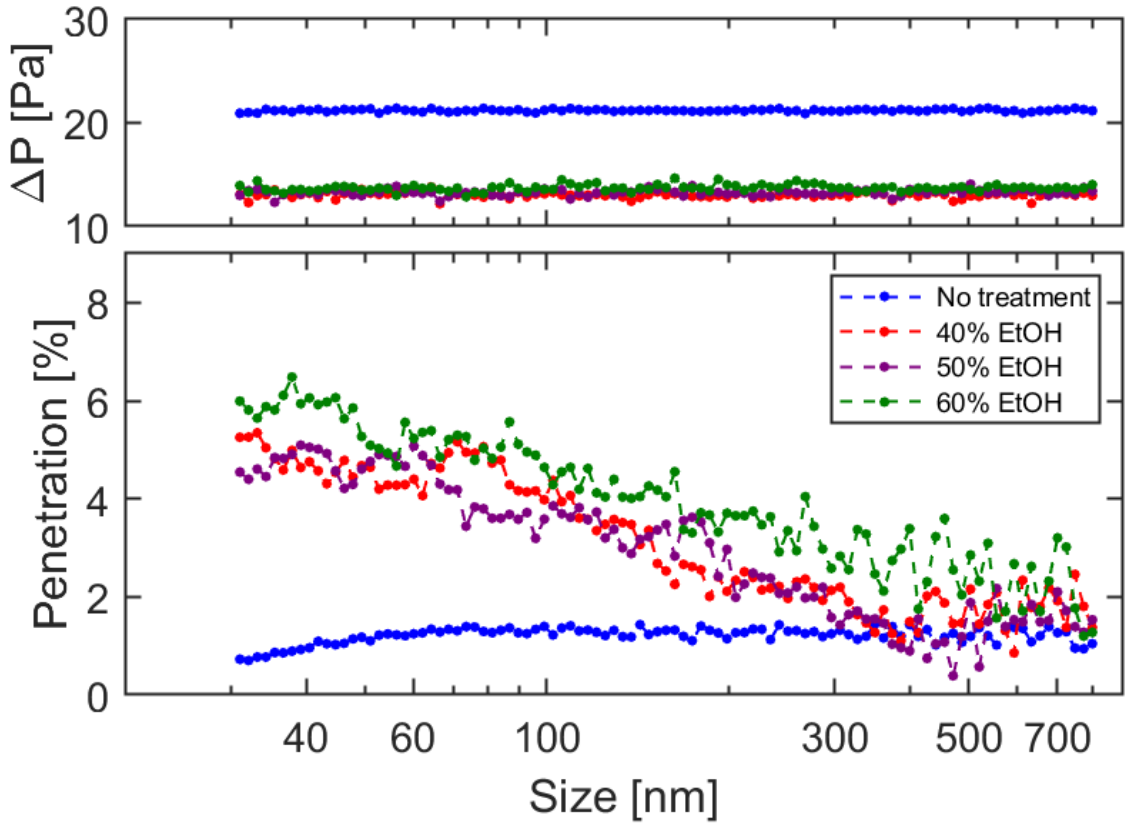

Figure 5.5. Penetration vs aerosol particle diameter for different liquid treatments of 3M 8210 N95 respirators. Figure courtesy of Buddhi Pushpawela and the Flagan group.

The filtration efficiency data, while preliminary, appears to agree with the wetting and discharge theory developed in chapter 2, the wetting experiments of chapter 3, and the TSD results from chapter 4. Finally, the polarization calculated through the TSD current appears to be related to the filtration efficiency of the respirators, but this relationship does not appear to be linear: the removal of ~2/3 of the polarization (40%, 50%, 60%, 62.4% EtOH w/w) resulted in ~3% of filtration damage while complete discharge (100% EtOH) resulted in ~7% of filtration damage.

Chapter VI: Conclusions

A theory of liquid-induced discharge of polymer microfiber electret filters was developed in this thesis. The theory was tested by a series of wetting, TSD, and filtration experiments on polypropylene microfiber electret filters from 3M 8210 N95 respirators. The results from these experiments support the idea that liquid-induced discharge of polymer microfiber electret filters is caused by the location of the solid-liquid interface in the filter. For a nonwoven network of rough microfibers, this solid-liquid interface can be either: resting on the outside of the filter, resting on the surfaces of all the microfibers, or on and inside all the microfibers. Transitions between these three interface locations, for soaked samples, are dependent on the surface tension of the applied liquid, the surface free energy (SFE) of the solid, and the roughness of the individual microfibers. Due to the low conductivities of the polymers used in these filters, the solid-liquid interface can only remove charge from the microfibers up to a certain depth, and thus the three possible locations of the solid-liquid interface correspond to three separate electret states in the polymer microfibers. Likewise, these microfiber electret states determine the electrostatic collection efficiency of the filter.

5.1 Applicability of Results and Theory

While the experimental work in this thesis focused on a single example of a polymer microfiber electret filter, the results of this work are likely generalizable to other polymer microfiber electret systems. For example, the wetting experiments of chapter 3 strongly suggest that the low filtration damages reported in the literature for polypropylene microfiber electret filters treated with dilute bleach, 3-6% hydrogen peroxide, and water (Fig. 1.1) are the result of those liquids never entering the filters. This filter wetting should occur spontaneously if the liquid surface tension is at or below the SFE of the polymer, but as dilute bleach, 3-6% hydrogen peroxide, and water all have high surface tensions, this is most likely not the case.

While this first solid-liquid interface transition (from outside to inside the filter), should just depend on the polymer (through its SFE), the second solid-liquid interface transition (from the microfiber surface to penetrating the microfibers) is presumed to depend on the manufacturer through the resulting roughness of the individual microfibers. Additionally, the specifics of discharge by any solid-liquid interface should also be manufacturer dependent with fiber diameter, porosity, and electret structure all presumed to play a role. Differences in these parameters can probably explain the wide distribution of filtration damages reported in the literature for polypropylene microfiber electret filters treated with low surface tension solutions (Fig. 1.1). Finally, as several filters in Fig. 1.1 appeared to withstand the low surface tension treatments, there is probably a set of fiber parameters that is resistant to liquid-induced discharge.

5.2 Future Work

The discharge theory developed in this thesis should be tested using additional liquids and different filters. In particular, the effect fiber diameter and porosity have on the discharge should be investigated. If it is true that the solid-liquid interface only discharges the first layer of trapping sites near the interface, then the different wetting regimes of a microfiber electret could provide a novel method to quantify the distribution of the electret state in the fibers.

Finally, more filtration data needs to be collected so that the polarization of the 3M 8210 N95 microfibers can be correlated to the electrostatic collection efficiency of the filter.

References

[1] Kravtsov, A., et al. “The Electret Effect in Polypropylene Fibers Treated in a Corona Discharge.” *Advances in Polymer Technology*, vol. 19, no. 4, 2000, pp. 312–316., doi:10.1002/1098-2329(200024)19:4<312::aid-adv7>3.0.co;2-x.

[2] Baumgartner, H-P., and F. Löffler. “The Collection Performance of Electret Filters in the Particle Size Range 10 Nm-10 Mm.” *Journal of Aerosol Science*, vol. 17, no. 3, 1986, pp. 438–445., doi:10.1016/0021-8502(86)90126-6.

[3] 3M Corporation. “3M Particulate Respirator 8210, N95.” *Technical Specification Sheet*, 3M Corporation, 2018, multimedia.3m.com/mws/media/1425070O/3m-particulate-respirator-8210-n95-technical-specifications.pdf.

[4] Sessler, Gerhard Martin. “Physical Principles of Electrets.” *Electrets*, by Gerhard Martin Sessler, Second ed., Springer, 1987, pp. 1–75.

[5] Viscusi, Dennis J, et al. “Effect of Decontamination on the Filtration Efficiency of Two Filtering Facepiece Respirator Models.” *Journal of the International Society for Respiratory Protection*, vol. 24, 2007, pp. 93–107.

[6] Bergman, Michael S., et al. “Evaluation of Multiple (3-Cycle) Decontamination Processing for Filtering Facepiece Respirators.” *Journal of Engineered Fibers and Fabrics*, vol. 5, no. 4, 2010, p. 155892501000500., doi:10.1177/155892501000500405.

[7] Xiao, Huiming, et al. “Correlation between Charge Decay and Solvent Effect for Melt-Blown Polypropylene Electret Filter Fabrics.” *Journal of Electrostatics*, vol. 72, no. 4, 2014, pp. 311–314., doi:10.1016/j.elstat.2014.05.006.

[8] Lam, Tu-Ngoc, et al. “Multi-Scale Microstructure Investigation for a PM2.5 Air-Filter Efficiency Study of Non-Woven Polypropylene.” *Quantum Beam Science*, vol. 3, no. 4, 2019, p. 20., doi:10.3390/qubs3040020.

[9] Liao, Lei, et al. “Can N95 Respirators Be Reused after Disinfection? How Many Times?” *ACS Nano*, vol. 14, no. 5, 2020, pp. 6348–6356., doi:10.1021/acsnano.0c03597.

[10] Ou, Qisheng, et al. “Evaluation of Decontamination Methods for Commercial and Alternative Respirator and Mask Materials – View from Filtration Aspect.” *Journal of Aerosol Science*, vol. 150, 2020, p. 105609., doi:10.1016/j.jaerosci.2020.105609.

[11] Grillet, Anne M, et al. “COVID-19 Global Pandemic Planning: Performance and Electret Charge of N95 Respirators after Recommended Decontamination Methods.” *Experimental Biology and Medicine*, vol. 246, no. 6, 2020, pp. 740–748., doi:10.1177/1535370220976386.

[12] Janssen, Larry L, et al. “Efficiency of Degraded Electret Filters: Part I – Laboratory Testing Against NaCl and DOP before and after Exposure to Workplace Aerosols.” *Journal of the International Society for Respiratory Protection*, vol. 20, 2003, pp. 71–80.

[13] Vazquez, Gonzalo, et al. “Surface Tension of Alcohol Water + Water from 20 to 50 .Degree.C.” *Journal of Chemical & Engineering Data*, vol. 40, no. 3, 1995, pp. 611–614., doi:10.1021/je00019a016.

[14] Enders, Sabine, et al. “Surface Tension of the Ternary System Water + Acetone + Toluene.” *Journal of Chemical & Engineering Data*, vol. 52, no. 3, 2007, pp. 1072–1079., doi:10.1021/je7000182.

[15] Guerisoli, Danilo M.Z., et al. “Evaluation of Some Physico-Chemical Properties of Different Concentrations of Sodium Hypochlorite Solutions.” *Physico-Chemical Properties of Hypochlorite Solutions*, University of São Paulo, 1998, www.forp.usp.br/restauradora/Trabalhos/prnaclo.html.

[16] Phibbs, M. K., and Paul A. Giguère. “HYDROGEN PEROXIDE AND ITS ANALOGUES: I. DENSITY, REFRACTIVE INDEX, VISCOSITY, AND SURFACE TENSION OF DEUTERIUM PEROXIDE – DEUTERIUM OXIDE SOLUTIONS.” *Canadian Journal of Chemistry*, vol. 29, no. 2, 1951, pp. 173–181., doi:10.1139/v51-022.

[17] Adamec, V. “The Volume Resistivity of Electrical Insulating Organic Materials under Irradiation.” *The International Journal of Applied Radiation and Isotopes*, vol. 15, no. 8, 1964, pp. 477–483., doi:10.1016/0020-708x(64)90075-4.

[18] Thyssen, Anders. “Charge Distribution and Stability in Electret Materials.” *Technical University of Denmark*, DTU Nanotech, 2016.

[19] Brière, G B. “Electrical Conduction in Purified Polar Liquids.” *British Journal of Applied Physics*, vol. 15, no. 4, 1964, pp. 413–417., doi:10.1088/0508-3443/15/4/310.

[20] Kumikov, V. K., and Kh. B. Khokonov. “On the Measurement of Surface Free Energy and Surface Tension of Solid Metals.” *Journal of Applied Physics*, vol. 54, no. 3, 1983, pp. 1346–1350., doi:10.1063/1.332209.

[21] Kernaghan, Marie. “Surface Tension of Mercury.” *Physical Review*, vol. 37, no. 8, 1931, pp. 990–997., doi:10.1103/physrev.37.990.

[22] Lee, Lieng-Huang. “Relationships between Surface Wettability and Glass Temperatures of High Polymers.” *Journal of Applied Polymer Science*, vol. 12, no. 4, 1968, pp. 719–730., doi:10.1002/app.1968.070120410.

[23] Bonnerup, C., and P. Gatenholm. “The Effect of Surface Energetics and Molecular Interdiffusion on Adhesion in Multicomponent Polymer Systems.” *Journal of Adhesion Science and Technology*, vol. 7, no. 3, 1993, pp. 247–262., doi:10.1163/156856193x00691.

[24] Whyman, Gene, et al. “The Rigorous Derivation of Young, Cassie–Baxter and Wenzel Equations and the Analysis of the Contact Angle Hysteresis Phenomenon.” *Chemical Physics Letters*, vol. 450, no. 4-6, 2008, pp. 355–359., doi:10.1016/j.cplett.2007.11.033.

[25] Brakke, Kenneth A. “The Surface Evolver Version 2.70 August 25, 2013.” *Surface Evolver*, facstaff.susqu.edu/brakke/evolver/evolver.html.

[26] Princen, H.M. “Capillary Phenomena in Assemblies of Parallel Cylinders.” *Journal of Colloid and Interface Science*, vol. 34, no. 2, 1970, pp. 171–184., doi:10.1016/0021-9797(70)90167-0.

[27] Beebe, A. H., et al. “Equilibria in Ethanol-Water System at Pressures Less Than Atmospheric.” *Industrial & Engineering Chemistry*, vol. 34, no. 12, 1942, pp. 1501–1504., doi:10.1021/ie50396a019.

[28] GmbH, DDBST. “Vapor-Liquid Equilibrium Data.” *Vapor-Liquid Equilibrium Data of Ethanol + Water from Dortmund Data Bank*, www.ddbst.com/en/EED/VLE/VLE%20Ethanol%3BWater.php.

[29] GILES, C. H., and A. H. SOUTAR. “Surface Tension of Ionised Dye Solutions.” *Journal of the Society of Dyers and Colourists*, vol. 87, no. 9, 2008, pp. 301–304., doi:10.1111/j.1478-4408.1971.tb03029.x.

[30] Sessler, Gerhard Martin. “Thermally Stimulated Discharge of Electrets.” *Electrets*, by J Van Turnhout, Second ed., Springer, 1987, pp. 81–201.

[31] Samuels, Robert J. “Quantitative Structural Characterization of the Melting Behavior of Isotactic Polypropylene.” *Journal of Polymer Science: Polymer Physics Edition*, vol. 13, no. 7, 1975, pp. 1417–1446., doi:10.1002/pol.1975.180130713.

[32] Keithley. “Model 6487 Picoammeter/Voltage Source Reference Manual.” *6487 Picoammeter Specifications*, Tek.com, Mar. 2011, download.tek.com/manual/6487-901-01(B-Mar2011)(Ref).pdf.

Appendix A: TSD Data Analysis

A.1 Peak Polarization Calculation

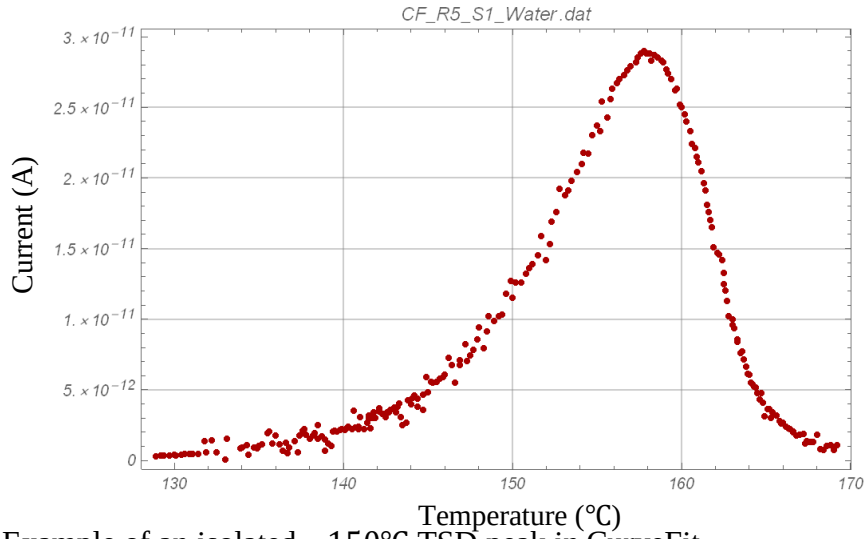

Figure A.1. Example of an isolated ~150℃ TSD peak in CurveFit.

The data from each TSD spectrum was loaded into the CurveFit Mathematica package and the ~150℃ TSD peak was isolated (Fig. A.1). The initial and final temperatures of the peak were recorded, and the times corresponding to these temperatures were used as the limits in the numerical integration of the TSD peak via equation 4.2. Integration of the TSD current was done in excel using the trapezoidal rule, and the final polarization value was obtained by dividing the integration result by the cross-sectional area of the filter sample (as eq. 4.2 is for a current density).

There were two sources of error considered in the error estimates for the polarization. The first error source originated from the accuracy of the Keithley 6487 picoammeter and was estimated from the specification sheet as a 500 fA current offset [32]. The second source of error considered was from inaccuracies in the areas of the polypropylene filter samples. These errors were modeled as a $\pm$1mm uncertainty in the radius of the samples. This uncertainty in the sample area came from inaccuracies in cutting and from the wrinkling and slight curvature of the filter samples.

A.2 Activation Energy Calculations

Activation energy was calculated for each TSD spectrum through analysis of the isolated ~150℃ TSD peak in CurveFit (Fig. A.1). For the FWHM method, the temperatures corresponding to the peak maximum and half-maxima were recorded. The activation energy was then calculated via equation 4.7. Uncertainty in the activation energy was not calculated for the FWHM method.

For the initial rise method, only the first 10% of the current rise was analyzed. The logarithm was taken of this data, and this was plotted against inverse temperature (in 1/Kelvin). The data was then linearly fit, and activation energy was calculated by multiplying the slope by the Boltzmann constant and flipping the sign (eq. 4.6). The activation energy uncertainty was

calculated in a similar manner by using the uncertainty in the slope of the fit. Figure A.2 shows this procedure carried out on the peak seen in Fig. A.1.

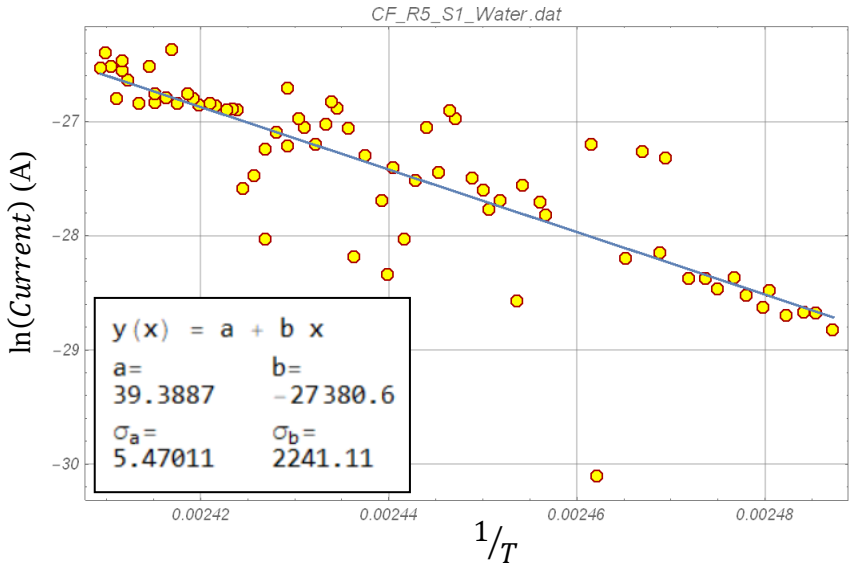

Figure A.2. Example fit for the activation energy. This plot is referred to by van Turnhout as a *Bucci-Fieschi* plot [30]. The activation energy of this peak was $2.36 \pm 0.19\ eV$ calculated through the initial rise method and $3.38\ eV$ through the FWHM method.